

A Metallicity Snapshot of the Small Magellanic Cloud from Spectra of RR Lyrae Stars

Anders Nyholm

Faculty of Engineering, LTH
Lund University

and

Lund Observatory
Lund University



2013-EXA72

Degree project of 30 higher education credits (for a degree of Master)
January 2013

Lund Observatory
Box 43
SE-221 00 Lund
Sweden

A Metallicity Snapshot of the Small Magellanic Cloud from Spectra of RR Lyrae Stars

Anders Nyholm

Examensarbete för avläggande av civilingenjörsexamen i teknisk fysik.
Thesis for the Degree of Master of Science in Engineering Physics.

Supervisor:

Dr Thomas Bensby
Lund Observatory
Lund University

Examiner:

Professor Ragnar Bengtsson
Division of Mathematical Physics
Faculty of Engineering, LTH
Lund University

Abstract

Using spectra of RR Lyrae stars in the Small Magellanic Cloud (SMC) a metallicity snapshot from an early epoch in the history of the SMC could possibly be obtained. The SMC, one of our closest neighbours in the Local Group of galaxies, offers the opportunity to study another galaxy close-up. The history of the SMC can be traced using the chemical characteristics of its different generations of stars. The early history of the SMC is debated, and it would be desirable to determine a metallicity distribution function (MDF) of such old ($\sim 10^{10}$ years) stars as the RR Lyrae variables in the SMC.

This work uses low resolution RR Lyrae spectra extracted from images obtained in September 2005 with the IMACS spectrograph and camera (in multislit mode) on the 6.5 m Magellan I telescope in Chile. By measuring the equivalent widths of the Balmer γ and δ lines from hydrogen and the Ca II K line from calcium and using Andrew Layden's method, the metallicity of the SMC RR Lyrae stars could be determined.

Multislit spectroscopy of RR Lyrae stars in the SMC with a 6.5 m telescope proved to be a challenge – only 4 stars in the images showed spectra of sufficient quality for a metallicity determination to be made. The metallicities were found to be in the range expected for RR Lyrae stars, but no MDF could be constructed. In the years since 2005, other groups have had more success studying the MDF of RR Lyraes in the SMC via photometric methods, and their work is briefly reviewed here along with some ideas for future studies.

Contents

1	Introduction	3
2	Background	3
2.1	The Big Picture: Our Galaxy and the Magellanic Clouds	3
2.2	The stellar life cycle	8
2.3	The history and evolution of the Small Magellanic Cloud	9
2.4	RR Lyrae stars	10
2.5	Astronomical spectroscopy and elemental abundances	12
2.6	The CCD in astronomy	15
3	Observations	15
3.1	The selection of observing targets	15
3.2	Observations from the Magellan I telescope	16
4	Data reduction	17
4.1	Using IRAF to extract spectra	17
4.2	Available image files and results of the reduction	19
5	Metallicity determination of RR Lyrae stars	20
5.1	The method of Layden	20
5.2	Using the Layden method on this dataset	23
5.3	Other methods: Clementini or Wallerstein	24
6	Results	25
6.1	[Fe/H] of the Milky Way, M 22 and SMC RR Lyrae stars	27
6.2	Discussion	28
6.3	Comparisons with other work	32
6.4	Future work	33
7	Summary and conclusions	34
8	Acknowledgements	35
	References	36
9	Appendices	39
9.1	Appendix 1: Supplementary images	39
9.2	Appendix 2: Supplementary method descriptions	41
9.3	Appendix 3: Supplementary tables	43
9.4	Appendix 4: A simple model of a pulsating star	44
10	Populärvetenskaplig sammanfattning på svenska	46

1 Introduction

This thesis addresses questions about the history of our cosmic neighbourhood – more specifically, the early history of the Small Magellanic Cloud, one of our nearest neighbouring galaxies. The history of the Small Magellanic Cloud can be investigated by studying its chemical evolution. The chemical differences between different generations of stars, and the importance of these differences for understanding the history of e.g. a galaxy, will be described in the background section. An important aspect of chemical evolution is that later generations of stars contain more heavy elements than earlier generations. The work presented here concerns observations of a type of star with variable brightness, called RR Lyrae star, which represent a stellar population with a minimum age of $\sim 10^{10}$ years. The study of RR Lyrae metallicities thus offers a snapshot of the metallicity distribution of the Small Magellanic Cloud at an early stage of its history.

The metallicities of the RR Lyrae stars will be examined by using the abundance of iron the stars as a proxy for their metal content. The iron abundance will be determined from stellar spectra obtained with the IMACS spectrograph and camera on the 6.5 m Magellan I telescope in Chile. The abundance will be determined via the study of spectral lines of hydrogen and calcium, which, through a method developed by Andrew Layden, can be used to find the iron abundance. The original aim of the work was to obtain the distribution of metallicities for the RR Lyrae stars studied. Increased knowledge about the history of the Small Magellanic Cloud is worth striving for, since this close neighbour of ours in intergalactic space offers unique opportunities to study another galaxy in detail and gain insight into how galaxies evolve. Recent observational studies of the star formation history of the Small Magellanic Cloud differ in their conclusions about the early history of the Cloud, and a successful study of its old stellar population is desirable.

This thesis has three major parts. First, the material presented in section 2 is written so that a physicist without special knowledge in astronomy shall be able to get a sense of the background of the problem and the means used to investigate it. Second, sections 3 through 7 describe the observational material and the methods used to determine the metallicities, ending with a discussion of the results and suggestions for future work. Third, the appendix section contains supplementary material such as examples of the routine for image processing.

2 Background

2.1 The Big Picture: Our Galaxy and the Magellanic Clouds

A clear night, far from disturbing light sources, offers an impressive view of the sky. Apart from phenomena in the atmosphere of the Earth such as aurora and meteors, objects in the solar system such as planets and the occasional bright comet, and apart from the individual stars, a diffuse and somewhat cloud-like band can be seen stretching across the sky. In English, this band is called the Milky Way. A perceptive sky watcher might notice that more bright stars are visible in or close to the band compared to fur-

ther from it. Early use of the telescope, at the beginning of the 17th century, revealed the the cloud-like band consisted of large numbers of faint stars, impossible to resolve with the unaided eye. In the late 18th century William Herschel made systematic star counts across the sky, concluding that the Milky Way as a stellar system has a flattened shape and that the Sun is situated in its centre. While the notion of the Milky Way having a flattened shape is correct, the erroneous view that the Sun sits at the centre of the Milky Way survived into the 20th century. By studying the distribution across the sky of globular clusters (densely packed clusters of old stars orbiting the Milky Way), Harlow Shapley concluded in the 1910s that the Sun can not be situated in the centre of the Milky Way. See e.g. Bensby (2004). The position of the Sun (cf. Figure 1) explains why more bright stars can be seen inside and close to the Milky Way band in the sky: The Milky Way appears as a band in the sky since it is a disk that we view from the inside, and when we look along the plane of this disk there is a higher probability to see a luminous and/or nearby star than when looking out of the disc.

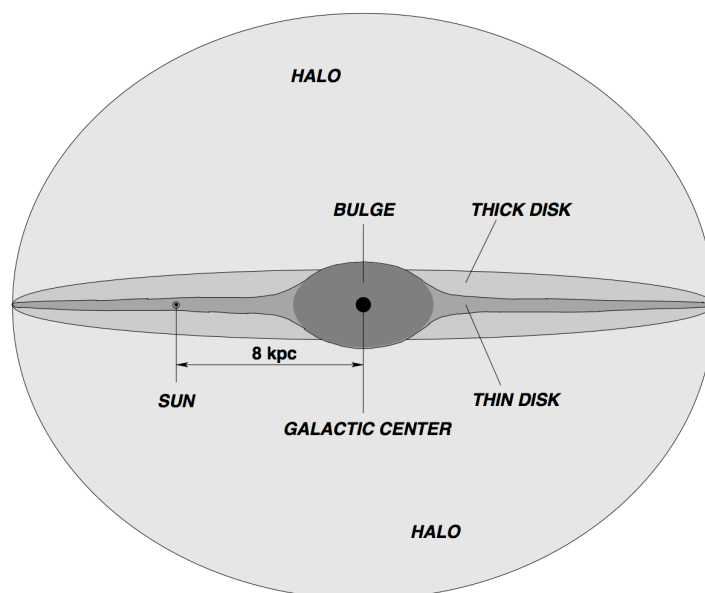


Figure 1: The main parts of the Milky Way, seen edge-on.
Figure from Bensby (2004).

The work of Edwin Hubble, Knut Lundmark and others around 1920 led to the discovery that the Milky Way is but one of many galaxies in the universe and that the universe is expanding (cf. Steer (2012)). For his distance measurements, Hubble used a type of variable star, called Cepheids, with a known relation between absolute brightness and the period of change in brightness. By studying Cepheids in the Andromeda nebula (as it was then known), commonly believed to be a part of the Milky Way, Hubble could determine that the Andromeda nebula was located well outside the Milky Way – and thus a galaxy of its own, one among many. A more detailed account of the history of

Milky Way studies can be found in chapter 1 of Matteucci (2001). The Milky Way is now known to have a diameter of approximately 35 kpc¹, and it contains $\sim 10^{11}$ stars. It is located in the so-called *Local Group* of galaxies, which has a diameter of $\gtrsim 3$ Mpc and contains over 50 galaxies, the most massive members being the Milky Way and the Andromeda galaxy. From here on the Milky Way will be referred to as the Galaxy, with a capital G.

Studying the Galaxy from our position inside it is a challenge, not least due to the interstellar dust and gas obstructing the view, but the following picture has emerged: The Galaxy is an oblate disc with spiral structure and with the highest concentration of stars towards the centre. The Sun orbits the centre of the galaxy at a distance of approximately 8 kpc, with an orbital period of about 200 million years. The visible constituents of the Galaxy are commonly thought to be made up of four major components (as described by e.g. Bensby (2004)): the thin and thick disks, the bulge and the stellar halo (see Figure 1). The *thin disk* is where most of the star formation in the Galaxy currently takes place, usually close to the galactic plane where gas and dust is abundant. Most of the stars in the thin disk are quite young, and have formed out of interstellar material that is rich in heavy elements. The *thick disk* surrounds the thin disk, and contains stars with a relatively large spread in velocities. Most investigators agree that the stars in the thick disk are old (ages $\gtrsim 7$ Gyr) and more metal poor than the Sun. The *bulge* surrounds the centre of the Galaxy, and is generally considered to consist of old stars, with a metallicity distribution peaking below the solar value, but also containing some young stars. The fourth, and least dense, stellar component of the Galaxy is the *stellar halo*, which is a spherical system of metal-poor stars orbiting the galactic centre in almost random orbits. The structure of the Galaxy is thus characterised by differences in chemical composition of the stars in the different parts, and the differences reflect the history of the Galaxy.

Two coordinate systems will be used in this work. (i) The *equatorial system*, where the coordinates are right ascension (α) and declination (δ). α is measured in hours, minutes and seconds eastward along the celestial equator from the vernal equinox; δ , the angular distance between the celestial equator and the object, is commonly measured in degrees, arc minutes and arc seconds. The celestial equator is a projection on the sky of the Earth's equator. (ii) The *galactic system* is based on the plane of the Milky Way in the sky, with longitude (l) measured in degrees eastwards from the direction towards the centre of the Galaxy (located in the constellation Sagittarius) and latitude (b) measured in degrees from the plane of the Milky Way in the sky.

Our Galaxy has a number of smaller companion galaxies in its neighbourhood. The two largest companions are the *Large* and *Small Magellanic Clouds*, located at distances of 50 kpc and 62 kpc, respectively. They are both small, irregular galaxies, visible to the unaided eye in the southern sky of the Earth. The Large Magellanic Cloud (LMC) can be seen at magnitude 1 on the border between the constellations Dorado (the Swordfish) and Mensa (the Table Mountain), whereas the Small Magellanic Cloud (SMC) can

¹A *parsec* (abb. *pc*) is a common unit of length in astronomy, corresponding to $3.0857 \cdot 10^{16}$ m.

be seen at magnitude 2 in the constellation Tucana (the Toucan; a tropical bird with conspicuous beak), 20° away from LMC in the sky.



Figure 2: The SMC photographed with a 300 mm f/5.6 lens. Celestial south is upwards. The bright star cluster to the left, 47 Tuc, lies at about $1/12$ of the distance of the SMC. Image © Stéphane Guisard, www.astrosurf.com/sguisard, used with permission.

The Clouds have been known to the inhabitants of the southern hemisphere for thousands of years, described in oral tradition. The Persian astronomer Abd al-Rahman al-Sufi, writing in Arabic, mentions the LMC in his *Book of the Fixed Stars* from around 964. This is possibly the earliest mentioning in writing of any of the Clouds. The Clouds came to wider attention in Europe through the southern sea voyages of Andrea Corsali, Peter Martyr d'Anghiera and Ferdinand Magellan in the early 1500s. In the pioneering star atlas *Uranometria* from 1603 – the first to cover the whole celestial sphere – by Johann Bayer, the Clouds are included and called *Nubecula Major* ("The Large Cloud") and *Nubecula Minor* ("The Small Cloud"). A popular designation for many years was *The Cape Clouds*, not least reflecting the importance of the commercial route around the Cape of Good Hope and how conspicuous the Clouds were to sailors going that way. The designation in use today refers to Ferdinand Magellan. Edmond Halley observed the Clouds during his astronomical expedition to St Helena in the 1670s, and in South Africa in the 1830s John Herschel made catalogues of objects in the Clouds (e.g. 244 objects in the SMC). The advent of photography and spectroscopy in the 19th century

was of great importance to astronomy, and the work of Henrietta Leavitt (studying photographic plates of the SMC) led to the publication in 1912 of the relation between absolute brightness and periods of the type of variable star known as Cepheids. This result proved to be of utmost importance when distances to other galaxies were to be determined (cf. Edwin Hubble, as mentioned earlier).

This concludes the overview of the early history of Cloud research (for more details, see Westerlund (1997)). A colourful account of the early cultural history of the Clouds can be found in *Kosmos* by von Humboldt (1874). At the time of writing (January 2013), the SIMBAD astronomical database lists over 6000 references for the SMC and over 9000 references for the LMC, so a description of the recent history of Cloud research is beyond the scope of this paragraph. As the literature about the Clouds is extensive, pp. 1500-1504 and 2426 in Murdin (2001) were used as background for this section.

Table 1: Location of the SMC in equatorial (α , δ) and galactic (b , l) coordinates.

α	δ	$b(^{\circ})$	$l(^{\circ})$	Distance (kpc)
00h 52m 44s	$-72^{\circ} 49.7'$	302.7969	-44.2992	62 ± 6

The LMC is larger than SMC both apparently and physically. Whereas the LMC covers about $7^{\circ} \times 7^{\circ}$ in the sky, has a physical extension of about 6 kpc and a mass² of $\sim 10^{10} M_{\odot}$, the SMC occupies about $4^{\circ} \times 3^{\circ}$ in the sky, has an extension of about 4 kpc and a mass of $\sim 10^9 M_{\odot}$. The location of the SMC³ is specified in Table 1. The SMC is stretched into an elongated shape, but its extension perpendicular to the plane of the sky is debated. The long axis of the SMC is pointing towards our Galaxy, presumably a result of tidal forces exerted by the Galaxy. As described by Subramanian & Subramanian (2012), the SMC has a bar (though less pronounced than the bar of the LMC), and an eastern extension called the Wing. A feature shared by the two Clouds is the *Magellanic Bridge*, a band of neutral hydrogen linking the SMC and LMC. The SMC contains substantially less gas and dust than the LMC, but the SMC nonetheless contains significant numbers of HII regions (areas with large amounts of ionised atomic hydrogen), young stellar clusters and young, hot stars. These features suggests a recent period of star formation (see section 2.3), possibly triggered by a close encounter with the Galaxy. The motion of the Clouds have been subject to much study (see e.g. van der Marel et al. (2008) and references therein), and studies have suggested both that the Clouds are following open orbits (passing the Galaxy for the first time) or closed orbits (with suggested orbital periods on the order of $\sim 10^9$ years). If the SMC has not formed in the vicinity of our Galaxy, but perhaps at some other place in the Local Group, this

²For convenience, the mass of the Sun ($1.9891 \cdot 10^{30}$ kg), designated M_{\odot} , is often used as the unit of mass in astronomy.

³Obtained in January 2013 from the NASA/IPAC Extragalactic Database (NED) at <http://ned.ipac.caltech.edu>.

could possibly be revealed through studies of old stars in the SMC.

2.2 The stellar life cycle

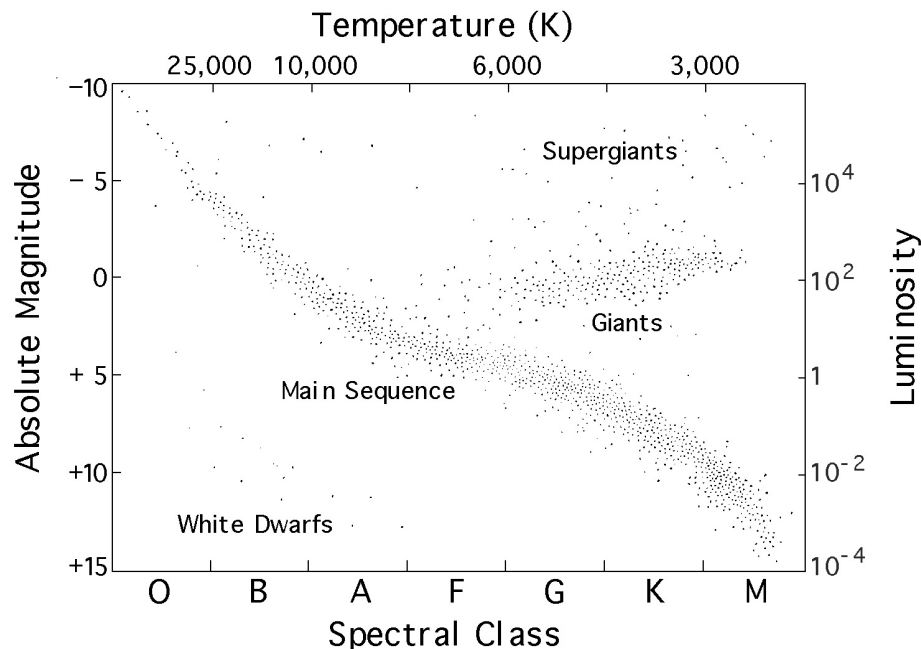


Figure 3: The HR diagram. Luminosity is given in solar units ($1 L_{\odot} = 3.839 \cdot 10^{26} \text{ W}$). The magnitude scale is logarithmic, such that a difference of 5 magnitudes corresponds to a factor of 100 in brightness. Figure courtesy of NASA.

Stars are formed out of the interstellar medium, i.e. out of the gas and dust in the space between the stars. The longevity of a star is primarily governed by its mass. Stellar mass is also the key to how a star will end its life. The basic mechanisms governing a star are mechanical and thermal equilibrium. This requires, among other things, that the inward gravitational pull is balanced by the differential pressure force caused by the thermal motion of the gas inside the star. If this, and other, requirements are fulfilled, the star remains stable. A star spends most of its life maintaining this stability, but as the end of the star's life approaches and this stability is disturbed, different scenarios can occur. An important tool for understanding stars and stellar evolution is the Hertzsprung-Russell (HR) diagram. Such a diagram (Figure 3) shows the the luminosity (or absolute magnitude) plotted against temperature (or colour) of a star, and when a large sample of stars is plotted, some distinct patterns appear. The most conspicuous pattern is the so called Main Sequence (MS), where a star spends its life as long as its stability is maintained. A star of a mass similar to or somewhat larger than the Sun's will spend $\sim 10^{10}$ years on the MS, then move away from the MS and become a red giant star and eventually eject its outer gas layers towards the end of its life, leaving behind a

compact stellar remnant known as a white dwarf (with Earthlike size and Sunlike mass). More massive stars ($\gtrsim 8 M_{\odot}$) consume their fuel faster and live for $\lesssim 10^7$ years, then explode as supernovae and leave behind even more compact objects, such as neutron stars or black holes. A neutron star may contain a solar mass within a radius of 10 km, being extremely degenerate. A black hole, being the most extreme stellar end-product, is so compact that not even light (according to classical physics) can escape it. The gas ejection by lighter stars and the supernova explosions of heavier stars thus enrich the interstellar medium with heavy elements.

Let us consider the role of the chemical elements in stars. The isotopes present in the newly formed universe were hydrogen (^1H), deuterium (^2H), helium (some of the ^3He and most of the ^4He) and some lithium (^7Li). The primordial mass fractions were $X \simeq 0.75$ for hydrogen, $Y \simeq 0.25$ for helium and $Z \simeq 0.00$ for the other elements. In this notation, $X + Y + Z = 1$. An overview can be found in chapter 1 of Pagel (2009). Elements heavier than helium are often referred to as "metals" in astronomy.

Some of these heavy elements have been formed inside the stars through the process of thermonuclear fusion, which is the source of energy of a star. In such a reaction, lighter atomic nuclei are fused into heavier nuclei. The high temperature and high pressure in the core of a star ($\sim 10^7$ K and $\sim 10^{16}$ Pa, respectively, in the core of the Sun) allows the energies of the positively charged nuclei to be sufficiently high to overcome the repulsive forces between them. When nuclei lighter than iron are fused, binding energy is released, and this constitutes the energy source of a star. Elements heavier than iron are formed under different conditions, such as during energetic and short-lived events as supernova explosions. As giant stars that end as supernovae have short lives, the interstellar medium is frequently enriched by heavier elements. Younger stars must, as a consequence, contain more heavy elements than older stars. This section on stellar evolution is based on chapters 10 and 11 of Karttunen et al. (2007).

As an example of how metals are more abundant in more recent generations of stars, such as the Sun, the solar mass fractions, as given in Table 7 of Lodders et al. (2009), $X = 0.7390$, $Y = 0.2469$ and $Z = 0.0141$ can be compared to the post-Big Bang fractions given above to see that chemical evolution has taken place.

2.3 The history and evolution of the Small Magellanic Cloud

Being two of the closest galaxies, the Magellanic Clouds are among the best-studied galaxies. As such, they serve as benchmarks in topics such as stellar populations and chemical evolution. In his monograph about the Magellanic Clouds, Bengt Westerlund wrote that "*The past history of the Magellanic Clouds is still veiled in obscurity.*"⁴ Progress has been made, however. A study (Harris & Zaritsky, 2004) of the star formation history (SFH) of the SMC has been made using photometry of more than $6 \cdot 10^6$ SMC stars, with the Cloud divided into 351 subregions to give a spatially resolved SFH. The investigators suggest a SFH of the SMC divided into 3 epochs: *i.*) An early epoch (more

⁴p. 21, Westerlund (1997)

than 8.4 Gyr ago) when a significant fraction ($\sim 50\%$) of the stars in the SMC formed. *ii.*) An intermediate epoch between 3 and 8.4 Gyr ago when relatively few stars were formed in the SMC. *iii.*) The most recent epoch, less than 3 Gyr ago, there has been continuous star formation punctuated by bursts at 2.5 Gyr, 400 Myr and 60 Myr.

Observations of the SMC by Sabbi et al. (2009) with the Hubble Space Telescope have been used for studying the SFH of the SMC. Among their conclusions are that the SMC formed stars already about 12 Gyr ago, albeit with a slow initial star formation rate; they argue against Harris & Zaritsky (2004) who claim that lively star formation took place in the SMC early on. Sabbi et al. (2009) also claim star formation activity has increased in the recent past (less than 0.5 Gyr ago) and that SMC stars younger than about 0.8 Gyr are confined to the bar and wing of the galaxy. This conclusion about recent star formation seem to match the results of Harris & Zaritsky (2004), but the disagreement about the early history of the SMC stresses the need for study of the old stars in the galaxy – e.g. the RR Lyrae stars and their metallicities.

2.4 RR Lyrae stars

At an occasional glance, the stars in the night sky might seem static, of never changing brightness. More careful observation, however, reveals that some stars actually change in brightness as time passes. For some stars, such changes can even be seen with the unaided eye. In fact, stars with varying light output are common, and there are different mechanisms causing the variations. One type of variability is caused by radial pulsation of the star, caused by internal instabilities. The type of variable star of interest in this work is a type of pulsator called RR Lyrae variable. This RR Lyrae overview is mainly based on chapter 6.11 in Percy (2007) and chapter 1 in Smith (1995). The type is named after the prototype star, RR Lyrae, which – at a distance of about 260 pc and an apparent magnitude around 7.5 (within reach of binocular viewing) – happens to be the closest and apparently brightest such star in the sky.

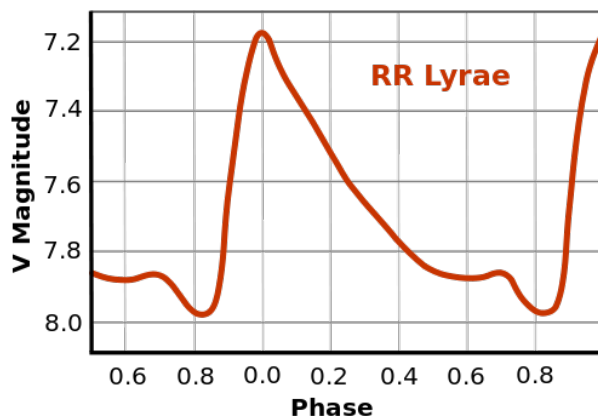


Figure 4: The folded light curve of RR Lyrae, as a representative example of a RRL light curve. Maximum brightness occurs at phase 0. Public domain figure. Creative Commons.

RRL⁵ stars are characterised by the properties of its variability: The period of variability is usually 0.1 to 1 day, the amplitude in magnitudes usually 0.2 to 1.5 (cf. Figure 4). RRL stars are also defined by their evolutionary state and their location in the HR diagram. They are stars which are thought to have begun as low-mass ($0.8M_{\odot}$) stars on the MS, burning hydrogen in its cores. Eventually, after $\sim 10^{10}$ years, the hydrogen supply at the core becomes exhausted, and the star begins to burn helium in their core instead. Stars in this stage of evolution have a narrow range of luminosities but a wide range of temperatures and therefore occupy a so called *horizontal branch* in the HR diagram (cf. Figure 3). If their temperatures lie between 6000 and 7500 K, they are unstable against pulsation. Another way to describe this condition is to say that if the star falls within the boundaries of the so called *instability strip* on the HR diagram, the star pulsates. The RRL phase of a star's life has a limited duration. As the central helium is depleted, after $\sim 10^8$ years, the star leaves the horizontal branch, swells and cools, becoming a red giant.

The ionisation of helium holds the key to how the pulsations of a RRL star are driven. As the star contracts, the density and temperature of the layer of He II (first He ionisation) in the star increases and this helium undergoes another ionisation, into He III (doubly ionised helium). This increases the opacity of the star and the flux of energy from the star's interior is effectively blocked. The temperature of the star increases and it starts to expand. During the expansion, the He III begins to recombine to He II and the opacity decreases. This decreases the temperature of the star, and the star starts to contract. The cycle then starts anew. This description is a simplification, but captures the essentials of the physics involved. The period of the pulsation can be estimated in a simple way, as demonstrated in the appendix (section 9.4). It can be noted that mass is very unequally distributed in a RRL star. The dense core has a radius of about 5 Earth radii and a mass of about $0.5M_{\odot}$, while the outer 50 % of the star's radius can contain as little mass as $\sim 0.001M_{\odot}$.

RRL stars as a group are very homogeneous, in every respect but in their metal abundance Z . Whereas the hydrogen abundance is $X \simeq 0.75$ and the helium abundance is $Y \simeq 0.25$, the abundance of heavier elements Z can be anywhere between 0.01 and 0.00001 (in terms of fraction of stellar mass). The RRL stars are important from a chronological point of view, when populations of stars are studied. Considering the conditions necessary for a RRL star to pulsate, the very existence of RRLs in a stellar population indicates that the population is older than 10 Gyr. A study of a sample of RRLs in e.g. a star cluster or galaxy gives the *Metallicity Distribution Function* (MDF) of the cluster or galaxy at an early stage in its history ($\sim 10^{10}$ years ago), integrated over earlier epochs, since the RRLs formed around that time. This circumstance will be used in this work.

⁵For the sake of brevity, "RR Lyrae" will be written as RRL in what follows.

2.5 Astronomical spectroscopy and elemental abundances

Spectroscopy, in the widest sense of the word, concerns the mapping of energy levels in a physical system. In astronomy, where electromagnetic radiation is the most important source of information, spectroscopy deals with the amount of light of different wavelengths reaching us from astronomical objects. The development of astronomy since the 19th century has shown us that spectroscopy has provided more information about the stars than any other technique. Spectroscopy has provided means to study, among other things, the composition, temperature, rotation and magnetic fields of stars.

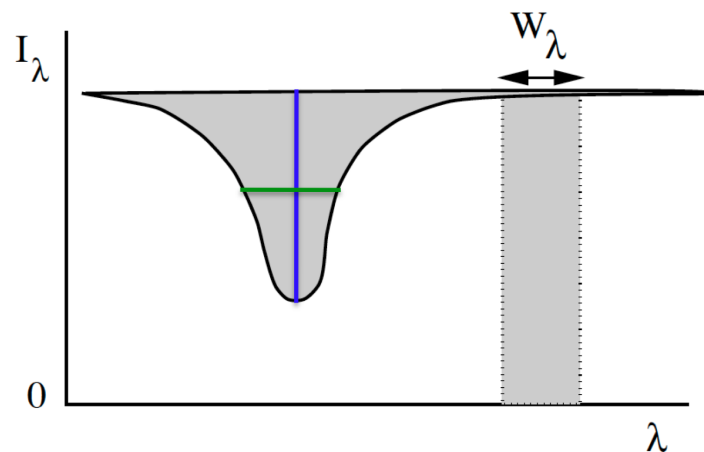


Figure 5: The equivalent width (here: W_λ) of an absorption line. The horizontal, green bar inside the spectral line indicates the line width and the vertical, blue bar indicates the line depth. Figure courtesy of Nils Ryde.

The spectra studied in this work are absorption spectra originating at the surfaces of RRL stars. The absorption spectra arises when the continuum radiation from inside the star passes through the star's outermost layers (known as the photosphere), where light from the continuum radiation is absorbed at specific wavelengths determined by the elements present in the photosphere. Each element has a certain electron structure and therefore absorb light at wavelengths characteristic of that element. This description is somewhat crude, but captures the essence of the process.

When an absorption spectrum is plotted with wavelength on the x-axis and intensity on the y-axis (see e.g. Figure 14), a curve with pronounced dips in it can be seen. The dips are the absorption lines, and they have widths determined by various conditions. The strength of a spectral line is characterised by its so-called *equivalent width*, later to be abbreviated *EW*. The equivalent width (W_λ in Figure 5) is the width of a rectangle with the same area as the total area of the absorption line and a height determined by the continuum. A question central to the background of this work is: *How does the abundance of an element in a star affect the equivalent width of a spectral line in the spectrum of that star?*

This can be understood by means of the *curve of growth*. A curve of growth is a relationship between the effective number of absorbing atoms in a stellar photosphere and the intensity of a spectral line in an absorption spectrum. This kind of plot can be used to estimate relative abundances of different chemical elements in a star. A qualitative description will be offered here, but details about the curve of growth are given in e.g. chapter 3.2.2 in Pagel (2009). For a popular introduction, see Robinson (2007). The basics of the curve of growth can be understood as follows:

Imagine a layer of gas (such as a stellar photosphere) containing atoms of a certain element, being irradiated by light. At low number densities of our element, the absorption line from the element would deepen as the number of atoms increase. That is, as we increase the number density slightly, the EW of the line also increases. At sufficiently low number densities, this increase is linear. Eventually, the number of atoms would be high enough to saturate the line. This means that the EW will not increase even if the number density of atoms is increased. However, if the number density is increased even further pressure broadening (due to emitted radiation being affected by nearby particles) of the line start occurring. Pressure broadening allows the wings of the line to develop, and this allows the EW to grow even further. A plot of the EW as a function of the number of absorbing atoms is called the curve of growth. For an example, see e.g. Figure 13.11 in Gray (2005).

The description is not complete, though. Contrary to the example above, the number density of an element can not be changed in a stellar photosphere. In the photosphere, some atoms will be ionised and some neutral. Furthermore, different atoms will occupy different energy levels and all atoms will therefore not absorb light – another condition is that different transitions in the atom has different probabilities of occurring, and this is measured by the so called *oscillator strength*, designated f .

To perceive how different properties of the photosphere and the atoms of interest affects the curve of growth, consider the curve (for a weak spectral line) as expressed in equation 1 (originally equation 16.4 in Gray (2005)):

$$\log \left(\frac{W}{\lambda} \right) = \log C + \log A + \log g_n f \lambda - \theta_{ex} \chi - \log \kappa_\nu \quad (1)$$

The EW, here written as W , is divided by the wavelength λ to normalise Doppler-dependent phenomena such as Doppler broadening, caused by the thermal motion of the atoms. The constant C contains information about the fraction of ionised atoms of the element in question. A gives the abundance of the element relative to hydrogen, the product $g_n f \lambda$ handles transition probabilities (g_n being the statistical weight associated with the energy level and f the oscillator strength), θ_{ex} represents the temperature of the photosphere and χ is the excitation potential for the energy level and κ_ν is an absorption coefficient of the photosphere. The dependence of the EW on the elemental abundance can then be understood as follows: A certain spectral line has fixed $g_n f \lambda$ and χ , and a model of the photosphere gives θ_{ex} and κ_ν . This leaves the EW depending on

the relative abundance A . This is a simplification, and today most theoretical abundance determinations are done with numerical models of stellar atmospheres producing synthetic spectra against which observations can be compared. The above description hopefully gives an idea of how the elemental abundance affects the spectral lines.

Elemental abundances in astronomy are usually treated according to a logarithmic convention. The Sun is used as a reference when chemical abundances are discussed in astronomy. The following relation applies for the number density N_E of the atoms of element E , the number density N_H of hydrogen atoms and the abundance $A(E)$ of the element E :

$$\log A(E) = \log_{10} \left(\frac{N_E}{N_H} \right) + 12.00 \quad (2)$$

A practical reason for adding the number 12.00 in equation 2 is that negative abundance values are avoided in most cases. As an example, let us consider the abundance of iron, which is commonly used as a proxy for overall metallicity. Table 4 in Lodders et al. (2009) gives that the abundance of iron in the solar photosphere is $\log_{10} A(\text{Fe}) = 7.45$. This gives the logarithm of the number of iron atoms per hydrogen atom as $\log_{10} \left(\frac{N_{\text{Fe}}}{N_H} \right) = \log_{10} A(\text{Fe}) - 12.00 = 7.45 - 12.00 = -4.55$. This means that for every hydrogen atom in the solar atmosphere, we have $10^{-4.55} = 2.82 \cdot 10^{-5}$ iron atoms. Or, inversely, for every iron atom, we have $(2.82 \cdot 10^{-5})^{-1} \approx 35000$ hydrogen atoms.

The abundance of an element E in another star is related to the solar abundance of that element via equation 3. This equation relates the stellar abundance of the element to the solar abundance of the element (in both cases relative to hydrogen) in such a way that the solar abundance becomes 0.

$$[E/H] = \log_{10} \left(\frac{N_E}{N_H} \right)_{\star} - \log_{10} \left(\frac{N_E}{N_H} \right)_{\odot} \quad (3)$$

This is the abundance notation that will be used in this work. Let us, as an example, see what the stellar iron abundance of $[\text{Fe}/\text{H}] = -1.0$ means. We know from the example above that $\log_{10} \left(\frac{N_{\text{Fe}}}{N_H} \right)_{\odot} = -4.55$ for the Sun. Rewriting equation 3 gives us $\left(\frac{N_{\text{Fe}}}{N_H} \right)_{\star} = 10^{\left([\text{Fe}/\text{H}] + \log_{10} \left(\frac{N_{\text{Fe}}}{N_H} \right)_{\odot} \right)} = 10^{(-1.0 - 4.55)} = 2.82 \cdot 10^{-6}$ iron atoms per hydrogen atom for this star (or, inversely, 1 iron atom per 350000 hydrogen atoms).

By comparing with the previous example, we can see that $[\text{Fe}/\text{H}] = -1.0$ indeed means an iron abundance relative to the solar of $10^{-1.0} = 0.1$ (i.e. a factor of 10). In $[\text{Fe}/\text{H}]$ notation, the metallicities of RRL stars are commonly found in the interval from 0.0 to -2.5 (cf. Table 1.1 in Smith (1995)).

2.6 The CCD in astronomy

The use of *Charge-Coupled Devices* (CCDs) in astronomy was pioneered in the 1970s, and today they are ubiquitous for recording light in astronomy. A CCD is a semiconductor chip sensitive to light, subdivided into discrete areas (picture elements or *pixels*). The size of one pixel on the CCD used in this work is $15\ \mu\text{m}$ (IMACS, 2008). When a photon arrives at a pixel, a small electrical charge is generated and stored for later read-out. The CCD has several advantages over photographic film. The quantum efficiency (the fraction of incident photons which are detected) for a CCD can exceed 90 % for certain wavelengths (cf. $\approx 1\%$ for film). The dynamical range of a CCD (the ratio of brightness between the brightest and the faintest light source detectable) is typically $\sim 10^5$, which (according to how magnitudes are defined) corresponds to a difference of $100^{1/5} \cdot \log 10^5 \approx 12.5$ magnitudes. Within the dynamical range, the response of the CCD is essentially linear (unlike film): This means that the signal is proportional to the number of photons detected, making calibration straightforward. One circumstance limiting the size of a CCD chip is the time it takes to read out the registered light. To bypass this obstacle, CCDs used in astronomy are commonly mounted in mosaics of several chips, to allow larger fields of view to be imaged. The observations presented here were done with a $2 \times 4 = 8$ CCD chip mosaic, giving a total of 8192×8192 pixels as detecting surface (IMACS, 2008). More background can be found in e.g. Davenhall et al. (2001).

To make the images useful, it is necessary to make several types of CCD exposures when doing astronomical observations. A **bias frame** is an exposure of zero duration obtained when no light is incident on the CCD chip. A bias frame can be used to reveal electronic problems, such as noise in the CCD chip. A bias frame must not be mistaken for a dark frame, which is also obtained with no illumination, but with a certain exposure time. A **flat field frame** is obtained with light from a diffuse, even light source falling onto the CCD chip. The exposure time is such that mid-level pixel values are achieved. In the work presented here, light for flat fields comes from a halogen lamp reflected by a white screen. Flat fields reveal changes in sensitivity from pixel to pixel, and they can be used to compensate for such defects. See e.g. Davenhall et al. (2001). When spectroscopy is done, an image of **spectral arc lamps** are obtained through the same slitmask as the science image was obtained through. This is done to provide a wavelength scale for the science exposures (IMACS, 2008). The spectral lamp used for this work was a HeNeAr lamp, giving reference spectral lines from about $3900\ \text{\AA}$ to about $9660\ \text{\AA}$.

3 Observations

3.1 The selection of observing targets

The telescope time application for the observations used in this work is dated 14 April 2005 and has been given to me by Thomas Bensby (2012, private communication). It describes the selection of RRL stars from the OGLE II survey catalogue Soszyński et al.

(2002), and mentions that 571 RRL variables are evenly distributed across approximately 2.5 square degrees of the central parts of the SMC. The IMACS instrument, used for obtaining the images, has a field of view of 15.4×15.4 arc minutes (ca 0.25×0.25 degrees). It is argued in the telescope time application that one pointing of the Magellan I telescope and IMACS can capture approximately 20 RRLs, and observing eight fields in the SMC with IMACS should therefore yield spectra of ≈ 150 RRLs. This is about 25 % of the OGLE II sample. Table 2 gives details of the fields in SMC actually observed during the campaign. The numbering of the fields described reflects that not all planned fields were observed.

Table 2: Centres of fields observed in the SMC.

Field	α (h m s)	δ ($^{\circ}$ " ')	No. of RRLs
1	00 37 50	-73 42 18	13 RRLs
2	00 39 28	-73 20 24	17 RRLs
3	00 43 31	-73 03 16	17 RRLs
5	00 55 42	-73 11 11	22 RRLs

The selection of equivalent width standard stars was done from the stars in Table 6 in Layden (1994). The selected stars were HD 155967, HD 180482, HD 65925, HD 22413, BD -17 484 and Kopff 27. The reference RRL stars in the Milky way were chosen from a list by the same author (Table 7 in Layden (1994)) to be X Ari, DX Del, RX Eri, SV Eri and RR Cet to evaluate the metallicity determination method. A selection of 15 RRL in the globular cluster M 22 (NGC 6656) (chosen from Table 1 in Wehlau & Hogg (1978)) were also chosen to be observed.

3.2 Observations from the Magellan I telescope

The observations of RRL stars in the SMC presented here were made in September 2005 by Thomas Bensby and Sally Oey at the Magellan I telescope on the Cerro Manqui peak at Las Campanas Observatory in Chile. The Magellan I telescope, also called the Baade Telescope after astronomer Walter Baade, is a reflecting telescope with a 6.5 m paraboloid primary mirror of focal ratio (f ratio) 1.25. The telescope has a alt-azimuth mounting.

The instrument used during the observations is called IMACS (Inamori-Magellan Areal Camera and Spectrograph). This camera and spectrograph is permanently mounted on the Magellan I telescope, and is fed via the f/11 Gregorian secondary mirror of the telescope. IMACS has two cameras, with focal ratios f/2.5 and f/4.3, respectively, and here the f/4.3 mode was used.

Figure 6 shows the layout of IMACS, and the optical paths in the instrument. The light from the astronomical source enters from the left in the figure (at the f/11 focus of the telescope) passes through a collimator, is dispersed by the f/4 reflecting grating and is finally recorded by a CCD camera where a 8192 x 8192 pixel mosaic of 8 CCD chips

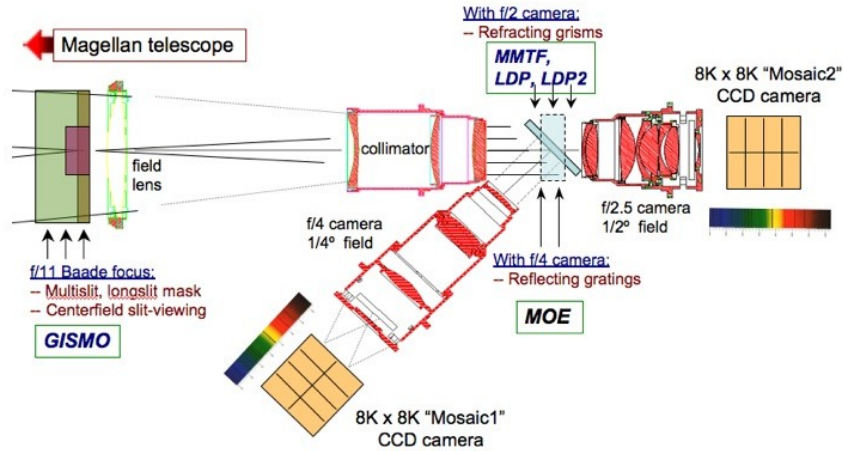


Figure 6: The layout of IMACS.
Figure from IMACS (2008).

serves as detecting surface.

For the current observations, a 300 lines/mm grating was used, providing a potential wavelength range of 3650 – 9740 Å. The estimated spectral resolution was $R = \lambda/\delta\lambda \approx 2700$. The observations were done in wide-field multislit spectroscopy mode, which means that an opaque mask of stainless steel is mounted at the f/11 telescope focus and that light from the astronomical sources passes through slits in this mask before entering IMACS. Multislit mode means that spectra of several objects can be recorded in one exposure. See Figure 13 in the appendix.

The images were obtained in the FITS (Flexible Image Transport System) format, which is widely used in astronomy. Each FITS file contains a header section with information about the image, such as exposure time, information about the instrumentation used, the pointing of the telescope etc. followed by the image data. Four different types of images were taken: bias, flat field, reference arc and science exposures. For a description of each kind of exposure, and for a motivation why it was taken, see section 2.6. Observations were done on three nights, September 25, 26 and 27, 2005 (UT). Four different fields in the SMC were observed, as well as the RRL in the M 22 globular cluster and the 11 different standard stars (EW standards and RRL stars).

4 Data reduction

4.1 Using IRAF to extract spectra

COSMOS (Carnegie Observatories System for MultiObject Spectroscopy) is a program especially written for processing data from IMACS. Thomas Bensby tried in 2005 to

use an earlier COSMOS version to process the images and to extract spectra from this observing campaign, but failed (probably due to problems with the wavelength calibrations). Initially, in this work, we intended to use a more recent version of COSMOS for the reductions. The program proved hard to install and compile, so we therefore decided to use IRAF (Image Reduction and Analysis Facility)⁶ instead. IRAF is a software system for processing and analysing astronomical images, and it is made up of a number of so called tasks. A task is a program for carrying out a certain part of the processing or analysis of an image, such as applying a flat field or extracting a spectrum. The IRAF tutorial by Walawender (2012) proved very useful when starting to extract the spectra. The routine for image processing and spectrum extraction is described in detail in an appendix (see section 9.2), but the main steps were the following:

1. **Making master versions of the bias images:** Bias images were combined into one master bias image per CCD chip.
2. **Making normalised, smoothed flat field images:** First, the bias was subtracted from all the flat fields and science exposures (but not the arc exposures). Then, all the bias subtracted flat fields for each field of view and chip were combined to produce master flat fields.
3. **Cropping, applying the flat field and removing cosmic rays from an image:** A considerable (10 - 30 pixels) and unexpected offset between the science exposures and the flat fields (and other calibration frames) had to be compensated for by cropping the flat fields and the science exposures in a suitable way before dividing the science exposure with the normalised flat field to obtain a normalised, flat fielded science exposure. This does not take out pixel-to-pixel variation but rather features that are a function of wavelength, e.g. fringing in the images. Finally, cosmic ray hits and other random pixel errors in the images were removed.

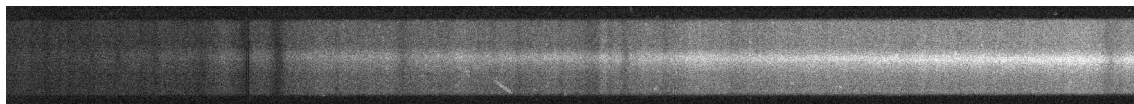


Figure 7: The extracted spectrum image of object 9 (my designation) on CCD chip 5 in field SMC3 on September 25, 2005. The broad grey band is background, while the narrow white strip is the dispersed light of the star (with OGLE II designation SMC_SC3_93692).

Having obtained a bias subtracted, flat fielded science exposure with cosmic ray hits removed, strips containing the spectrum from one object were copied out of the science exposure (see Figure 7), along with the accompanying arc exposure. The extraction of spectra and the application of a wavelength solution was later done as follows:

⁶IRAF is distributed by the National Optical Astronomy Observatories, which are operated by the Association of Universities for Research in Astronomy, Inc., under cooperative agreement with the National Science Foundation, USA. Revision 2.14 of IRAF, from November 2007, was used in this work.

1. **Indicating the direction of dispersion:** In order for IRAF to successfully extract a spectrum, the task for extraction must know the direction of spectral dispersion in the image. This is entered into the FITS header of image.
2. **Setting apertures for the spectrum and the background:** IRAF can display a window where it is possible to set apertures for the extraction of the spectrum, see Figure 8. One aperture is given where light from the astronomical object is present in the image, and other apertures are given for the background. The trace, i.e. the path followed by the aperture as one moves along the dispersion axis, is determined in a similar window.
3. **Generating a wavelength calibration solution:** The lines in the calibration lamp exposure must be associated with the wavelengths from a line list for the HeNeAr mixture. A window is displayed, showing the lines from the HeNeAr lamp, and by clicking on a the lines and entering their wavelengths from the line list, a wavelength solution can be constructed.

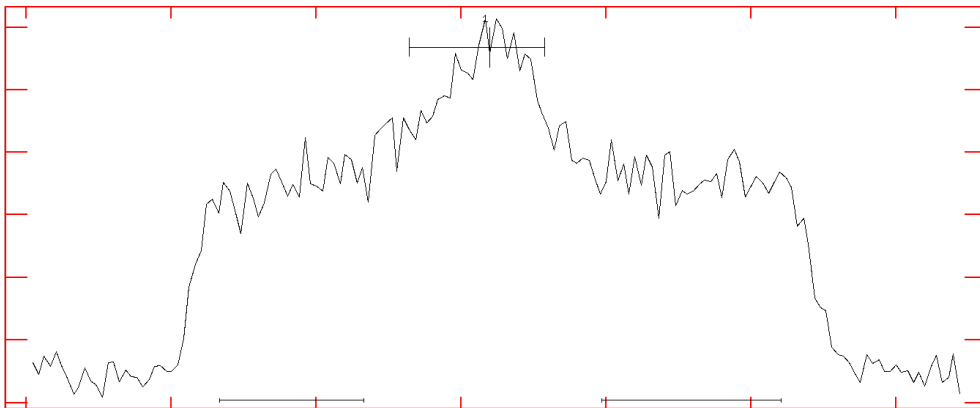


Figure 8: View along the dispersion axis of the extracted spectrum image in Figure 7. The black horizontal markings show where apertures for the object (peak in the middle) and background have been set. The x-axis shows location on chip (pixel coordinates) and the y-axis shows intensity (arbitrary scale).

The IRAF command `SPLIT` can be used to show a spectrum on the computer screen. In this mode a profile such as a gaussian or a lorentzian can be fitted to a spectral line, after points in the continuum surrounding the line has been marked. IRAF then determines the central wavelength of the line and its equivalent width (cf. Figure 15 in the appendix).

4.2 Available image files and results of the reduction

The number of images obtained during the observing campaign is given in Table 3. In the table, "EW" stands for equivalent width standard star spectra, "RRL" for local RRL stars spectra, "M 22" for spectra of M 22 RRL stars and "SMC" for SMC fields.

Table 3: Number of FITS images from Magellan/IMACS in September 2005.

Date (UT)	Bias frames	Arc frames	Flat fields	EW	RRL	M 22	SMC
September 25	10	13	85	3	2	0	3
September 26	0	6	113	2	4	1	3
September 27	9	6	58	1	5	1	3

The science exposures of the SMC fields and M 22 has exposure times of 40 minutes, the flat fields have exposure times of 2 or 5 seconds and the RRL and EW standard star spectra have exposure times of 10 – 60 seconds, depending on the star.

The image processing described in section 4.1 was applied to the images from the September 25 and September 26. As an example, a typical SMC field contains spectra of $\gtrsim 10$ objects, the spectrum of one object typically spread over 2-3 CCD chips. Manually reducing the images and extracting spectra with wavelength solutions took about 5 days per observing night. As the extraction of the spectra were made, it became apparent that the estimate of $S/N \approx 30$ (signal to noise ratio) made in the telescope time application was too optimistic. The typical S/N in the extracted spectra was usually in the range 3 – 10. The usefulness of the spectra was also questioned at this stage, since, in some cases, it was possible to discern one or two spectral lines but not more in the interesting (i.e. 3900 Å – 4900 Å) interval. In most cases, the spectra proved too noisy for anything of interest to be discerned. Due to time constraints and the low quality of the spectra, it was decided that the images from September 27 should not be processed. The measurements and analysis presented below is based on images from the first two nights, and the SMC fields 1, 2 and 3 (cf. Table 2), containing a total of 47 RRL stars.

A problem encountered when the wavelength solutions for the spectra were to be made was that there is a relative lack of HeNeAr lines in the area of interest, about 3900 Å – 4900 Å . Only 6 spectral lines are on the line list used⁷ for this wavelength interval, whereas the line density for the interval ca 5000 Å – 9600 Å is considerably higher. As the wavelength solution work progressed, the lines 3964.7289 Å and 4200.6745 Å from the <http://www.noao.edu/kpno/specatlas/> HeNeAr line atlas were eventually added to the list.

5 Metallicity determination of RR Lyrae stars

5.1 The method of Layden

In 1994, Andrew Layden published a study of the metallicities and kinematics of 302 nearby RRL stars in the Milky Way; see Layden (1994). Layden used the Ca II K, H δ , H γ and H β lines in the spectra of his RRL sample to determine the metallicities of these stars. The wavelengths in air of the lines⁸ are given in Table 4 and a typical

⁷Provided by Thomas Bensby (private communication, 2012).

⁸Wavelengths obtained from the NIST Atomic Spectra Database at <http://www.nist.gov/pml/data/asd.cfm>, October 2012.

RRL spectrum is shown in Figure 14 in the appendix. Note that the method uses a Ca line to determine Fe abundance; this will be commented on later. In the method, the pseudoequivalent width $E(W)$ of the Ca II K line is plotted against the mean EW of the H δ and H γ lines, $W(H)$.

Table 4: Spectral lines of interest.

Line	λ (Å)
H β	4861.35
H γ	4340.47
H δ	4101.73
Ca II K	3933.66

The pseudoequivalent width is measured in relation to the pseudocontinuum of the spectrum, which Layden defines as a straight line drawn between the mean intensity and the mean wavelength of continuum bands on either side of the spectral feature. A RRL star of a certain abundance describes a loop in the $E(W)$ - $W(H)$ (or so-called HK) plane as it goes through its pulsation cycle. A star observed in phase 0.0 – 0.8 (cf. Figure 4) will fall on a curve or line in the HK plane. In this plane, metal poor stars will lie below more metal rich stars.

A complication to this method is that a star in phase 0.8 – 1.0 (rising light) will have increased effective gravity at its surface and thus altered Balmer lines, so observations of stars at rising light must be identified and removed from the sample. If the epoch of the maxima of the observed stars is known, this can be used to remove unsuitable spectra. The pulsation limits the effective exposure time for a RRL star to about 40 minutes; for longer times, the star itself would change too much during the exposure.

Another complication comes from the absorption of light by interstellar calcium ions, which sometimes can make noticeable contributions to the Ca K absorption lines in RRL spectra. The size of the contribution depends on distance of the star and its location relative to the galactic plane. A third complication is the sensitivity of the H β line to the metal abundance of the star.

Due to these complications, Layden suggests an iterative method to determine the metal abundance. This method is based on the work of Ken Freeman and Alexander Rodgers; see reference in Layden (1994). The steps can be summarised as follows:

1. An estimate of the metal abundance $[\text{Fe}/\text{H}]$ is made using the uncorrected $W(\text{K})$ and the EW of the H δ and H γ lines.
2. The average apparent magnitude of the star is combined with an assumed relation between absolute magnitude and $[\text{Fe}/\text{H}]$ to estimate the distance of the star.
3. The absorption caused by the interstellar medium at this distance is estimated

using a model. The distance and the interstellar absorption is iterated until the absorption doesn't change.

4. A model for the interstellar calcium absorption is used along with the estimate of the star's distance and its galactic coordinates to estimate the contribution to the Ca K line from the interstellar medium.
5. The contamination of the $H\beta$ line is estimated in the same manner.
6. The metal abundance value is then recomputed based on the corrected values of $W(K)$ and $W(H)$.

Observed EWs of RRL stars with known $[Fe/H]$ are used to calibrate the HK plane, so measuring all the spectra in the same way should produce a consistent set of metallicities. The spectra themselves are not completely uniform, though, so the EWs needs to be transformed onto a common system. A set of radial velocity standard stars was used by Layden as EW standard stars. It can be noted that the EW of the $H\beta$ line depends weakly, but significantly, on the metallicity and Layden models this dependence. Layden presents a polynomial of the form

$$W(K) = a + b \cdot W(H) + c \cdot [Fe/H] + d \cdot W(H) \cdot [Fe/H] \quad (4)$$

with coefficients determined using observations of RRL stars with well known metallicities. Solving for $[Fe/H]$ gives

$$[Fe/H] = \frac{W(K) - a - b \cdot W(H)}{c + d \cdot W(H)} \quad (5)$$

In Table 5, the designation $W(K_0)$ for the Ca K equivalent width means that it is uncorrected for interstellar Ca contamination. $W(K)$ means that the EW of the Ca K line has been corrected for interstellar contamination. $H2$ means that only the $H\delta$ and $H\gamma$ lines are used when computing $W(H)$, so that

$$H2 = W(H) = \frac{W(H\delta) + W(H\gamma)}{2} \quad (6)$$

in this case.

Table 5: Coefficients of the Layden HK plane fits

Fit	a	b	c	d
$W(K_0)$ vs $H2$	13.542 ± 0.416	-1.072 ± 0.076	3.971 ± 0.285	-0.271 ± 0.052
$W(K)$ vs $H2$	13.669 ± 0.426	-1.125 ± 0.077	4.147 ± 0.291	-0.300 ± 0.053

5.2 Using the Layden method on this dataset

The Layden method as described above will not be used in this work. Since the distance to the observed as a fairly good approximation can be assumed the distance of the SMC, the iteration for determining the stellar distances will not be done here.

The interstellar contamination of the Ca K line inside the Galaxy was modelled by Beers (1990) as

$$W(K)_{interstellar} = \frac{W_{max} \cdot (1 - e^{-|z|/h})}{\sin |b|} \quad (7)$$

and the value $W(K)_{interstellar}$ obtained can be subtracted from the $W(K_0)$ value to get a corrected Ca K EW for use when calculating $[\text{Fe}/\text{H}]$. The parameters specified by Beers are $W_{max} = 0.192 \pm 0.008 \text{ \AA}$ (which is the total line strength of Ca K in the direction perpendicular to the galactic plane in a column extending to infinity) and $h = 1081 \pm 112 \text{ pc}$ which is a characteristic height (above the galactic plane) used to quantify the line strength data. The galactic latitude of the object of interest is designated b and z is the object's height above the galactic plane. For SMC we have $b = -44.3^\circ$ which (for a radial distance of 62 kpc) gives a distance to the galactic plane of $z = \sin 44.3^\circ \cdot 62 \text{ kpc} \approx 43 \text{ kpc}$. Using this distance and latitude in equation 7, with the parameter values of Beers, $W(K)_{interstellar} = 0.28 \text{ \AA}$ is obtained.

As a comparison, Borissova et al. (2004) (see section 5 in that paper) describes the use of the Layden method on RRLs in the LMC, and in their work no Ca K compensation is made. The fit shown in Figure 1 in Beers (1990) is interpreted here such that the model can be applied out to distances of about 60 kpc, and therefore use the model in my reductions to compensate for the Ca K in the Galaxy. The Ca K contribution in the SMC itself remains uncompensated for.

Another issue to consider when applying the Layden method in this work is how the EWs have been measured from the spectra. The EWs in the Layden dataset of standard stars were in most cases measured from several (often between 5 and 10) observations per star, whereas this material offered one spectrum per standard star to measure. In each spectrum, the task SPLOT in IRAF was used to mark two continuum points and fit a single line profile for measuring the EW of an absorption line. Since Layden used one method and this work uses another for measuring EWs for the same standard stars, it is relevant to see how the measurements presented here relate to Layden's. When the measurements are presented graphically, the Balmer EW measurements (figure 9, left panel) and the Ca EW measurements (figure 9, right panel) of Layden and of this work appear to relate linearly to one another. The linear least-square fits for $H\delta$ and $H\gamma$ in Figure 9 can be expressed as

$$W(H\delta)_{Layden} = 0.4298 \cdot W(H\delta)_{Nyholm} + 2.5792 \quad (8)$$

$$W(H\gamma)_{Layden} = 0.5407 \cdot W(H\gamma)_{Nyholm} + 1.8506 \quad (9)$$

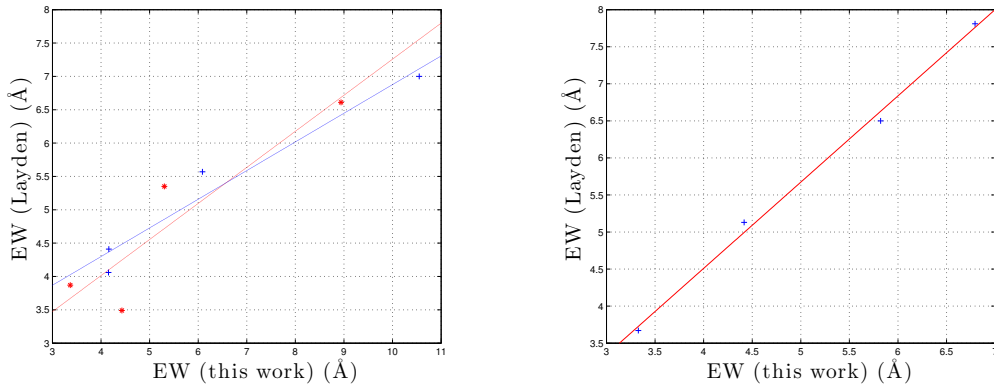


Figure 9: LEFT: The relation between the Balmer δ (+) and γ (*) EWs of Layden and of this work, for the EW standard stars BD-17484, HD22413, HD65925 and HD155967. RIGHT: The relation between the Ca EWs of Layden and the Ca EWs of this work for the same EW standard stars.

and the linear least-square fit for Ca K in Figure 9 can be expressed as

$$W(K)_{Layden} = 1.1640 \cdot W(K)_{Nyholm} - 0.1468. \quad (10)$$

These relations were used to adjust my measured RRL EWs to the Layden system before using equation (5) to make a metallicity estimate.

Layden also presents a third set of coefficients for his method (besides the two sets in Table 5), intended for use with the corrected Ca K line and the mean of the $H\beta$, $H\delta$ and $H\gamma$ lines. It is shown by Layden that the EW of the $H\beta$ depends weakly, but significantly, on the metallicity of the star. He presents a correction for the $H\beta$ metal contamination, but since the present spectra are noisy and of low resolution (so that the effect of any metal contamination is difficult to evaluate), the $H\beta$ lines and the metal correction is not used here.

5.3 Other methods: Clementini or Wallerstein

Other methods for determining the metallicity of a RRL star based on EWs of various spectral lines exist. A method suggested by Wallerstein et al. (2012) uses the EW of the Ca II line at 8498 Å in the Ca II infrared triplet and the relationship

$$[Fe/H] = -3.846(\pm 0.155) + EW_{8498} \cdot 0.004(\pm 0.0002). \quad (11)$$

This method is not applicable in this work since this absorption line cannot be seen in the available spectra. Others (Clementini et al., 1991) point out that the Ca K line is correlated with $[Fe/H]$ in RRL stars, and give the best-fit-relation

$$[Fe/H] = 0.53(\pm 0.09) \cdot EW_{corr} - 3.08(\pm 0.22). \quad (12)$$

It should be noted that this linear fit was made for stars observed at minimum light. In the Clementini relationship, the Ca EW used should be corrected for interstellar absorption. This correction can be made using the Beers model (Equation 7). The Clementini relationship will be used and the resulting abundances will be compared to the abundances given by the Layden method.

6 Results

This section presents the $[\text{Fe}/\text{H}]$ for the stars that it was possible to measure; a total of 3 standard RRL stars in the Milky Way, 4 RRL stars in the SMC and 2 RRL stars in M 22. In this section, the stars are identified with catalogue designations from the literature. During the data reduction informal designations were used, which meant giving each spectral trail in the FITS images a number. Files exist which describe the location of the slits in each slitmask, and by using these files it was possible to identify each star in the images. This identification was done after the extraction of the spectra, in order not to evoke any bias (e.g. through knowledge about the stars from catalogues) while spectral extraction was done.

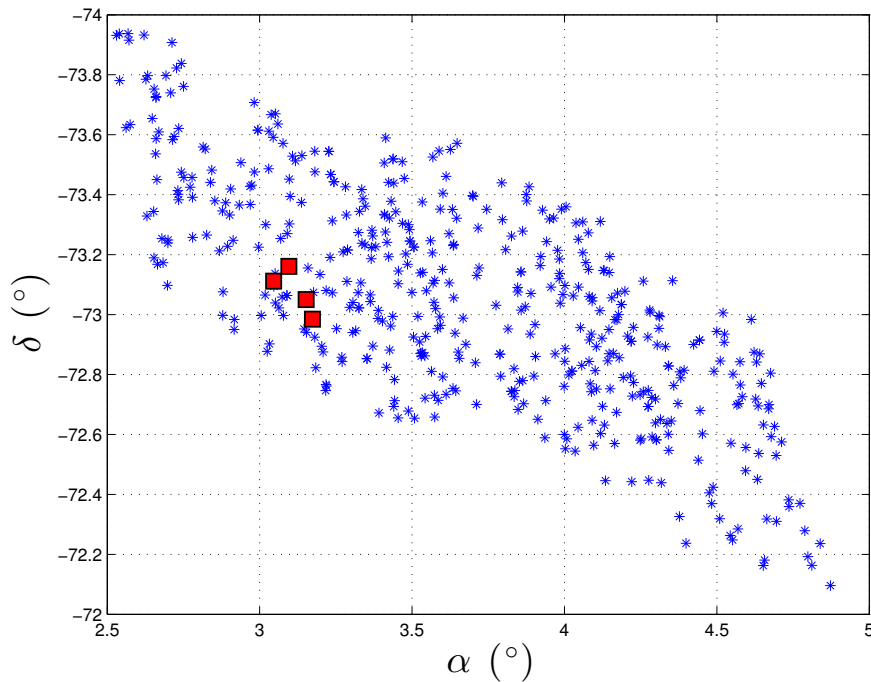


Figure 10: 448 RRLs in SMC, from the OGLE survey, plotted from a list based on Soszyński et al. (2002). The stars in Table 6 are marked as red boxes. Celestial south is upwards. The contours of the SMC can be discerned.

For Table 6 the phase Φ of the star (cf. Figure 4) was calculated using the epoch of the star (i.e. time of maximum brightness), the time of observation and the pulsation period of the star, using the formula⁹

$$\Phi = \frac{T_{\text{observation}} - T_{\text{epoch}}}{P_{\text{star}}} - \text{INT} \left(\frac{T_{\text{observation}} - T_{\text{epoch}}}{P_{\text{star}}} \right). \quad (13)$$

The epochs of the stars in Table 6 are given in HJD (Heliocentric Julian Days), which means a julian date corrected for the Earth's position in space with respect to the Sun. Due to the finite speed of light and the size of the Earth's orbit, the Earth can be several light minutes closer to or further away from an object outside the solar system than the Sun. A heliocentric reduction of observing times therefore helps obliterate the timing differences caused by the location of the Earth in its orbit. The difference between HJD and JD at the time of the observations¹⁰ was ca 2 minutes, whereas the exposure time of one image in this work is 40 minutes and the period of a RRL star is typically 0.2 - 1 day. The difference between JD and HJD is therefore neglected here.

Table 6: Observations of RRL stars in the SMC

Object	Exposure start (UT)	Exposure end (UT)	Period (d)	Epoch (HJD)	Phase (exp. start)	Phase (exp. end)
SMC_SC3_97657	2005-Sep-25 07:07:52	2005-Sep-25 07:47:52	0.3461943	2450621.66714	0.13	0.22
SMC_SC3_93692	2005-Sep-25 07:07:52	2005-Sep-25 07:47:52	0.6244510	2450621.50425	0.91	0.96
SMC_SC2_102160	2005-Sep-26 03:44:57	2005-Sep-26 04:24:58	0.5862976	2450625.47904	0.04	0.08
SMC_SC3_28949	2005-Sep-26 03:44:57	2005-Sep-26 04:24:58	0.3114067	2450626.76238	0.11	0.20

Periods and epochs obtained from the *OGLE-III On-line Catalog of Variable Stars* as described in Soszyński et al. (2010) via <http://ogledb.astrouw.edu.pl/~ogle/CVS/>. The designations of the objects are in OGLE II catalogue style.

Observations of RRL stars in M 22 were made as described in Table 7.

Table 7: Observations of RRL stars in M 22

Object	Exposure start (UT)	Exposure end (UT)	Period (d)	Epoch (HJD)	Phase (exp. start)	Phase (exp. end)
NGC6656_SAW_V6	2005-Sep-25 00:23:44	2005-Sep-25 01:03:44	0.638548	2442594.951	0.37	0.42
NGC6656_SAW_V15	2005-Sep-25 00:23:44	2005-Sep-25 01:03:44	0.37323	2442594.597	0.80	0.87

Periods and epochs from Wehlau & Hogg (1978).

Observations of standard RRL stars in the Milky Way were made as described in Table 8.

⁹Based on equation 3.2 in Percy (2007).

¹⁰Julian dates (JD) are a continuous count of days since noon Universal Time on January 1, 4713 BC. An estimate of the difference between JD and HJD for the SMC around the time of observing, i.e. late September 2005, can be obtained with the formula $\Delta T = JD - HJD = \frac{r}{c} \cdot [\sin(\delta) \cdot \sin(\delta_{\odot}) + \cos(\delta) \cdot \cos(\delta_{\odot}) \cdot \cos(\alpha - \alpha_{\odot})]$. For the position of the Sun in late September 2005 ($\delta_{\odot} \approx 0^{\circ}$, $\alpha_{\odot} \approx 12$ h) and the SMC ($\delta \approx -73^{\circ}$, $\alpha \approx 1$ h), with the Sun-Earth distance r approximated by the astronomical unit and c being the speed of light in vacuum, $\Delta T \approx 2$ minutes is obtained. Buchheim (2007), p. 270 gives the background of this calculation.

Table 8: Observations of RRL stars in the Milky Way

Object	Exposure start (UT)	Exposure end (UT)	Period (d)	Epoch (HJD)	Phase
SV Eri (1)	2005-Sep-25 09:32:23	2005-Sep-25 09:33:24	0.7137964	2453386.317	0.85
SV Eri (2)	2005-Sep-26 04:48:54	2005-Sep-26 04:49:24	--	--	0.98
X Ari	2005-Sep-26 04:57:52	2005-Sep-26 04:58:22	0.6511628	2453054.333	0.96
DX Del	2005-Sep-25 23:51:58	2005-Sep-25 23:52:58	0.47261673	2453181.507	0.04

Epochs for X Ari and DX Del were taken from Le Borgne et al. (2004), the epoch for SV Eri from Hübscher et al. (2005) and periods taken from Samus et al. (2012).

6.1 [Fe/H] of the Milky Way, M 22 and SMC RR Lyrae stars

Abundance values, [Fe/H], presented in this section were computed using EW measurements from the spectra with both the Layden and Clementini methods. The following procedure was used for the Layden method: **1.** The $H\delta$ EW was transformed for Layden method use with equation 8, as well as the $H\gamma$ with equation 9. **2.** The average of the $H\delta$ and $H\gamma$ EWs were calculated with equation 6. **3.** The Ca K EW was transformed for Layden method use with equation 10. The contribution from interstellar Ca contamination was calculated with equation 7 and subtracted from the result of equation 10. **4.** Using these processed EWs, the [Fe/H] abundance was calculated using equation 5 with the coefficients for "W(K) vs H2" from Table 5. The Layden method gives abundances on the metallicity scale of Zinn and West (see reference in Layden (1994)).

For the Clementini method, the corrected EW of the Ca K line from step 3 in the above list was used in equation 12 to obtain a [Fe/H] value.

When using the Beers model, the following values of galactic latitude $b(^{\circ})$ and distance r (kpc) were used – written here as (b, r) : SV Eri at $(-53.48, 0.64)$, X Ari at $(-39.83, 0.48)$ and DX Del at $(-18.85, 0.55)$ with latitudes from SIMBAD and distances from Layden (1994), M 22 at $(-7.55, 3.2)$ with values obtained via SIMBAD, and the SMC at $(-44.3, 62)$, with values from NED.

Tentative estimates of the errors are made by making three [Fe/H] computations per star and method. One computation using the coefficients, one using the coefficients minus the coefficient errors and one using the coefficients plus the coefficient errors.

The 3 RRL stars in the Milky Way for which spectra could be obtained and the equivalent widths measured are presented in Table 12 (appendix). The [Fe/H] for these stars, calculated with the Layden and Clementini methods, respectively, are presented in Table 9. The spectra of RX Eri and RR Cet were not possible to use.

Table 9: Calculated $[\text{Fe}/\text{H}]$ for the standard RRL stars in the Milky Way

Object	$[\text{Fe}/\text{H}]_{\text{Layden}}$	$[\text{Fe}/\text{H}]_{\text{Clementini}}$	Comment
SV Eri (1)	$-2.20^{+0.13}_{-0.21}$	-1.95 ± 0.03	Rising light
SV Eri (2)	$-2.28^{+0.19}_{-0.36}$	-2.41 ± 0.11	Rising light
X Ari	$-2.44^{+0.24}_{-0.45}$	-2.64 ± 0.14	Rising light
DX Del	$-0.67^{+0.32}_{-0.17}$	-0.50 ± 0.17	Past maximum

The 2 RRL stars in M 22 for which spectra could be obtained and the equivalent widths measured are presented in Table 13 (appendix). The $[\text{Fe}/\text{H}]$ for these stars, calculated with the Layden and Clementini methods, respectively, are presented in Table 10.

Table 10: Calculated $[\text{Fe}/\text{H}]$ for the objects in M22

Object	$[\text{Fe}/\text{H}]_{\text{Layden}}$	$[\text{Fe}/\text{H}]_{\text{Clementini}}$	Comment
NGC6656_SAW_V6	$-1.92^{+0.06}_{-0.09}$	-1.16 ± 0.10	Decreasing light
NGC6656_SAW_V15	$-1.23^{+0.05}_{-0.03}$	-0.01 ± 0.29	Increasing light

The 4 RRL stars in the SMC for which spectra could be obtained and the equivalent widths measured are presented in Table 14 (appendix). The spectra are presented in Figure 11. The $[\text{Fe}/\text{H}]$ for these stars, calculated with the Layden and Clementini methods, respectively, are presented in Table 11.

Table 11: Calculated $[\text{Fe}/\text{H}]$ for the SMC objects

Object	$[\text{Fe}/\text{H}]_{\text{Layden}}$	$[\text{Fe}/\text{H}]_{\text{Clementini}}$	Comment
SMC_SC3_28949	$-1.05^{+0.36}_{-0.13}$	-1.79 ± 0.00	Decreasing light
SMC_SC3_93692	$-0.34^{+0.38}_{-0.23}$	0.23 ± 0.34	Increasing light
SMC_SC3_97657	$-2.43^{+0.18}_{-0.29}$	-2.30 ± 0.09	Decreasing light
SMC_SC2_102160	$0.15^{+0.86}_{-0.42}$	-0.04 ± 0.30	Past maximum

The mean value and standard deviation of the SMC results from the Layden method are $\overline{[\text{Fe}/\text{H}]} = -0.99$ and $\sigma = 1.04$, respectively. For the values from the Clementini method, mean value and standard deviation are $\overline{[\text{Fe}/\text{H}]} = -0.96$ and $\sigma = 1.27$, respectively.

6.2 Discussion

The metallicities of the RRL stars in the Milky Way reported in Table 9 can be compared against values in the literature. In this way, the quality of the data and the usefulness of the analysis method can be evaluated. A compilation of $[\text{Fe}/\text{H}]$ for RRL stars in

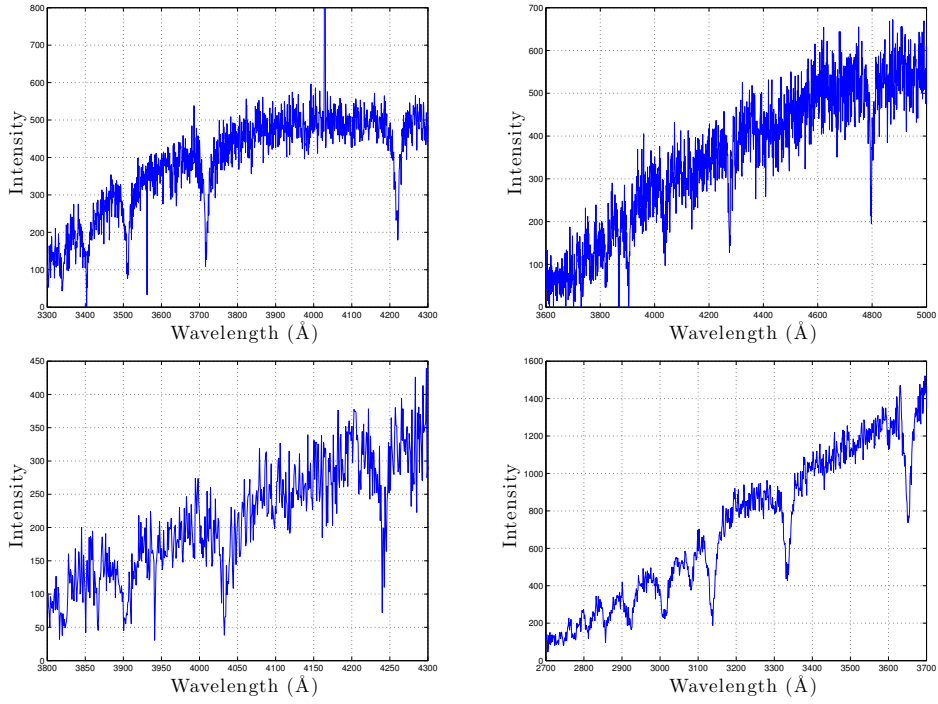


Figure 11: IMACS spectra of 4 RRL stars in the SMC. *From the top, left:* SMC_SC3_28949, SMC_SC3_93692, SMC_SC3_97657 and SMC_SC2_102160. The differences in wavelength intervals suggest problems with the wavelength calibrations. The intensity scales are arbitrary (based on pixel values on the CCD). For line identification, cf. Figure 14 in the appendix.

the Milky Way can be found in Feast et al. (2008), which gives $[Fe/H]_{DXDel} = -0.39$, $[Fe/H]_{SVEri} = -1.70$ and $[Fe/H]_{XAri} = -2.43$. The spectra of SV Eri and X Ari used in this work were taken during rising light (cf. Table 9), and should therefore be used with caution when metallicity is to be determined. My Layden metallicity for X Ari, $[Fe/H] = -2.44^{+0.24}_{-0.45}$, is quite in agreement with the value in Feast et al. (2008), but that could be a coincidence. My Clementini value for X Ari is lower than the literature value. However, the spectrum of DX Del was taken past maximum brightness, and ought to be more useful. However, the metallicity values obtained for DX Del, $-0.67^{+0.32}_{-0.17}$ (via Layden) and -0.50 ± 0.17 (via Clementini), are both lower than the literature value. My SV Eri metallicities (from both methods) are lower than the literature values, but it should be noted that the star was observed at rising light.

The use of outdated maximum epoch for the variables could affect the evaluation of the spectra, since the method of Layden delivers the best results for star outside the rising ($0.8 < \Phi < 1.0$) phase. Where possible, epochs recent at the time of observations (September 2005) have been used. However, this was not possible for the stars in M 22, and it is therefore hard to judge the quality of these $[Fe/H]$ determinations.

The age of the epochs (mid-1975) for the M 22 variables makes it hard to use the phases based on them for evaluation of the metallicity determinations. It is hard to calculate the time of maximum light for a RRL star based on an epoch several decades old. The timing of the maximum used could have deficiencies, and a small error in the decimals of the period is sufficient to cause a substantial error in the calculated phase via cumulative effects. The period changes of RRL stars (as understood from theoretical models) can be small for much of their life on the horizontal branch, but the observed period change rates can be larger¹¹.

The metallicity of M 22 is given by Marín-Franch et al. (2009) as $[Fe/H] = -1.80$ on the Zinn & West scale (used in this work). A globular cluster of stars like M 22 is commonly assumed to be old (age $\sim 10^{10}$ years), which is supported by the presence of RRL stars in the cluster, and of uniform and low metallicity. The star NGC6656_SAW_V6, which was possibly captured in decreasing light (cf. Table 10) has a metallicity determined as $[Fe/H] = -1.92$ with the Layden method. This happens to agree quite well with the metallicity of the entire cluster, but no useful conclusion can be drawn from one star alone. The star NGC6656_SAW_V15 was possibly captured during increasing light, and therefore results from the Layden and Clementini methods are not very useful.

There is a spread of wavelengths amounting up to $\sim 1000 \text{ \AA}$ in the measurements of the central wavelengths for the Balmer and Ca K lines, as can be seen in the tables in Section 6. The positions of the HeNeAr lines (as well as the calibration frames) have been shifted on the CCD chip. This is most probably caused by the handling of the slitmasks and other mechanical circumstances during the observations. If this kind of

¹¹Thanks to the members of the American Association of Variable Star Observers (AAVSO) online forum at <http://www.aavso.org/forum> for clarifying this and other issues related to RRL stars.

observation is about to be tried again, taking arc images before AND after each science exposure, and not (like in the observations presented here) just at one time before would be preferable.

The IMACS documentation (IMACS, 2008) gives the dispersion for the used 300 lines/mm grating as 0.743 \AA per pixel. Typical dispersions achieved in the wavelength solutions in this work is $0.73 - 0.75 \text{ \AA}$ per pixel, an interval covering the documentation value.

The HeNeAr gas mixture used to achieve reference lines for the spectra does not have many lines in the Ca II and Balmer area, around 4000 \AA . Another reference gas could possibly have been used. A Th + Ar mixture gives more lines, and could possibly improve wavelength calibrations.

The Clementini method is, according to its authors, devised for RRL spectra taken at minimum light. This could explain the high metallicity for SMC_SC3_93692 from the Clementini method, $[\text{Fe}/\text{H}] = 0.23$. This star was observed at rising light, which makes it unsuitable for the Clementini method.

The metallicity determined with the Layden method for SMC_SC2_102160, $[\text{Fe}/\text{H}] = 0.15$, is in itself too high to be reasonable for a RRL – the error of the determination seems to be quite large, however, and this star possibly has a metallicity of around 0.

Since the spectrum of SMC_SC3_97657 was obtained around phase 0.2, at decreasing light, and the Layden and Clementini determinations of $[\text{Fe}/\text{H}]$ agrees quite well (and the error estimate for the Layden determination for this star is quite small), this might be the star with the best determined metallicity in the sample. The spectrum of SMC_SC3_28949 was also obtained at decreasing light, and even though the difference between the Layden and Clementini determinations is larger, this star might have $[\text{Fe}/\text{H}] = -1.5$.

The Layden method can be interpreted as somewhat more robust, and useful for phases $0.0 < \Phi < 0.8$. However, the values of $[\text{Fe}/\text{H}]$ calculated with the Layden formula seem to be quite sensitive to the EWs measured in the spectra. An EW change of $\sim 0.1 \text{ \AA}$ can give quite large changes in the resulting $[\text{Fe}/\text{H}]$ value. With the Ca K line of SMC_SC3_28949 as an example (and the Balmer lines still as given in Table 14), the EW 2.149 \AA gives $[\text{Fe}/\text{H}]_{\text{Layden}} = -1.27$ and the EW 2.149 \AA gives $[\text{Fe}/\text{H}]_{\text{Layden}} = -0.83$. This difference, $\Delta[\text{Fe}/\text{H}] \approx 0.5$, demonstrated here by a change of $\pm 0.3 \text{ \AA}$ of the Ca K EW shows how sensitive the metallicity determinations are to changes in EWs.

The use of a calcium line to determine an iron abundance can appear indirect, but as pointed out by different investigators – see e.g. section 3 in Wallerstein et al. (2012), section 3.12 in Layden (1994) or sections 4 and 5 in Clementini et al. (1991) – there is a tight correlation between Ca line strengths and total metal abundance for RRL stars. However, the studies quoted all concerned RRLs in our Galaxy, but the stars actually observed for this study are located in the SMC. The SMC is another galaxy, with a different chemical history than ours and it is possible that the $[\text{Fe}/\text{H}]$ versus $[\text{Ca}/\text{H}]$ proportion in the SMC was different when the RRL stars formed.

Why did only a few stars give good spectra? All of the RRL stars in the sample have roughly the same apparent magnitude, so why did not all of them give good spectra (or all of them give noisy spectra)? Bad seeing, and changing seeing during the exposures, is probably the reason for this to a high degree. When the light of the stars falling into the slits of the mask is disturbed by changing seeing, light is lost and the S/N is lowered.

6.3 Comparisons with other work

During the years since 2005, when the observations treated in this work were done, fruitful work on RRL stars and metal abundances in the SMC has been made. A good example is the 2012 PhD thesis of Raoul Haschke: *Structure, Abundances, and Reddening of the Magellanic Clouds from its Variable Stars*.

A spectroscopic study of RRL metallicities (encompassing 3 stars) in the SMC is presented in Haschke et al. (2012b). This study is of special interest here since it used the companion telescope, Magellan Clay, of the telescope used in this work. However, the Haschke study was aimed at especially metal-poor RRL stars (albeit located in the eastern part of the SMC, like in this work), with $[\text{Fe}/\text{H}] < -2.0$. The most metal-poor RRL found by Haschke et al. in the SMC has $[\text{Fe}/\text{H}] = -3.41$. For these observations, the MagE spectrograph on the Magellan Clay telescope was used to obtain individual spectra with cumulative exposure times longer than in this work. A ThAr gas was used for reference lines. The individual exposure times were between 45 and 90 minutes, i.e. longer than the exposure times used here.

The study of Haschke et al. (2012a) encompasses 1831 RRL stars in the SMC, metallicities obtained through Fourier decomposition of light curves from the OGLE survey. A correlation exists between certain Fourier components of the light curve of a RRL star and the metallicity of the star (for an overview see e.g. Sandage (2004) and references therein). Such correlations have been used in many studies to determine RRL metallicities. The mean RRL metallicity found, on the scale of Zinn & West, is $[\text{Fe}/\text{H}] = -1.70 \pm 0.27$. The SMC is more metal poor than the LMC, where the corresponding mean RRL metallicity is found to be $[\text{Fe}/\text{H}] = -1.50 \pm 0.24$. The RRL metallicity distribution in both Clouds proved to be uniform, with no pronounced metallicity gradients visible.

Abundance data for RRLs in the SMC has also been extracted from the OGLE survey photometry by Kapakos et al. (2011). They present a set of abundance data that has been produced by Fourier decomposition analysis of OGLE RRL photometry. The result obtained for 100 RRL stars in the SMC by Kapakos et al. (2011) is shown in Figure 12, and has a peak around $[\text{Fe}/\text{H}] = -1.5$, as the metallicity distribution found by Haschke et al. (2012a) (cf. Figure 6 in that paper). It was a metallicity distribution function of this kind that was the original goal of this investigation.

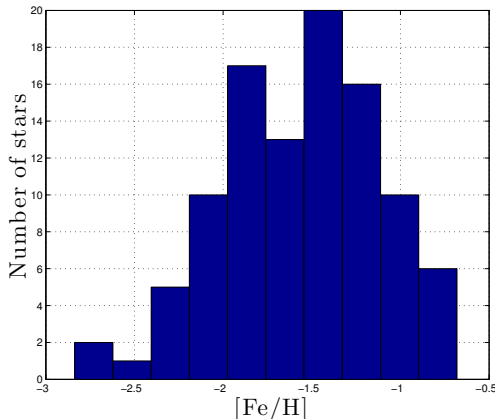


Figure 12: A histogram of the Kapakos et al. (2011) 100 RRL $[\text{Fe}/\text{H}]$ dataset for the SMC. Accessed via the VizieR Catalogue Service at <http://vizier.u-strasbg.fr> as *J/MNRAS/415/1366*.

A photometric study of RRL metallicities (encompassing 30 stars) in the SMC is presented by Baird et al. (2011). In the study, RRL stars in 2 fields in SMC were observed, and one of the fields (*Field 1* in the paper) is situated in the eastern part of the SMC, like the fields in this work. The weighted mean value of $[\text{Fe}/\text{H}]$ in Field 1 is reported to be -1.25 ± 0.15 , which is roughly comparable to the mean metallicity obtained for the 4 stars presented in Table 11.

6.4 Future work

The low S/N has been a major problem in the work presented here. How could a stronger signal be achieved? The stars themselves can not be changed – even though they are variable to some extent – and a RRL star in the SMC will always have an apparent magnitude of about 19. The pulsations of the stars do limit the exposure times possible. Using a larger telescope and thereby gather more light is one way to increase S/N. A rough estimate, by comparing the size of light gathering optics, shows that the planned 39 m European Extremely Large Telescope (E-ELT) will have a $(D_{ELT}/D_{Magellan})^2 \approx 36$ times as large light gathering area as the 6.5 m Magellan telescope used here. With this ~ 10 times increase in light gathering capacity, a repeat of the spectroscopy observations described here could possibly be more productive than when done with a 6.5 m telescope.

The OGLE IV survey has been running since March 2010, according to the project web site at <http://ogle.astrouw.edu.pl>. This version of the OGLE survey will study not only the SMC and the LMC but also the area of sky between the Clouds where the Magellanic Bridge is found. The OGLE IV survey should therefore provide an even larger dataset on RRL stars than the previous OGLE surveys, and better statistics can be achieved.

The ESA Gaia astrometry mission, slated for launch in 2013, will obtain positional

and radial velocity measurements for $\sim 10^9$ stars in the Galaxy, but also perform other studies. According to Bastian (2009), Gaia will be able to observe $\sim 10^6$ stars in the Clouds. In the case of RRL metallicity determinations, the method using the Ca II triplet suggested by Wallerstein et al. (2012) (see section 5.3) was developed with respect to the capability of Gaia to obtain spectra in a small spectral range where this feature can be found. A good dataset of RRL metallicities can be expected from the Gaia mission.

RRL stars have been studied in other galaxies. Both M 31 (the Andromeda galaxy) and M 33, two other major members of the Local Group, have had RRLs detected in them (cf. Smith et al. (2009)). Such detections are demanding, as RRL in M 31 have apparent magnitudes of about 25, but in the future more extensive studies of RRL stars in other galaxies than our Galaxy and the Clouds might be feasible.

On a personal note, it gives me a slight feeling of uneasiness that I have done all this work on the SMC without having seen it for myself. I should go to the southern hemisphere and see the SMC in person! ¹²

7 Summary and conclusions

The SMC, one of our closest neighbours in the Local Group of galaxies, offers the opportunity to study another galaxy close-up. The history of the SMC can be traced through the chemical characteristics of its different generations of stars, and while different groups have reached the conclusion that the SMC has undergone lively star formation recently, the earliest history of the galaxy is debated. The early epochs of a population of stars can be studied through RRL stars, which are metal-poor variable stars which have left the MS after $\sim 10^{10}$ years and spend a shorter period, $\sim 10^8$ years on the instability strip, pulsating. The presence of RRL stars in a stellar population indicates that the population is older than $\sim 10^{10}$ years, and the metallicity of the RRL stars represents that of the stellar population 10^{10} years ago, integrated over all older ages.

The aim of the observations described here has been to determine the metallicities of a number of RRL stars in the SMC in order to examine their metallicity distribution function. In September 2005, the IMACS spectrograph and camera on the 6.5 m Magellan I telescope in Chile was used for three consecutive nights to acquire low-resolution spectra of a sample of RRL stars in the SMC. After processing the raw images and extracting the spectra for two of the nights, the spectra proved to be not only of low resolution but also of low signal to noise ratio. Typical S/N of the spectra was between 3 – 10. Problems were also encountered when wavelength calibrations for the spectra were to be made. Andrew Layden’s method was used to determine the metallicities of the 4 RRL stars for which useful spectra could be extracted, and the 4 stars appeared to have

¹²In the summer of 2008, while working as a summer student at the Swedish Solar Telescope on La Palma (latitude 28.8° N), I challenged myself to see how far south I could see in the sky. η Arae at $\delta = -59^\circ$ was the southernmost star I was able to see and identify. At the declination of this star, 14° remains until the declination of the SMC is reached. Way to go!

metallicities in the range expected for RRLs. The errors of the determined metallicities were large, however, and the small sample not suited for any useful statistics.

The following conclusions can be drawn from this work:

- The RRL spectra extracted here are noisy (S/N usually between 3 and 10), and only 4 RRLs (out of 47 with extracted spectra) in the SMC were possible to measure in the way intended. Doing multislit spectroscopy of RRLs in the SMC with a 6.5 m telescope is a challenge, sensitive to the handling of the slit masks, the spectral reference arcs and to the seeing conditions while observing.
- The obtained metallicities for the 4 RRL stars in the SMC have large errors, but the $[\text{Fe}/\text{H}]$ values appear to lie mainly in the range where RRL metallicities are expected to be found: from 0.0 to -2.0 . The errors are large for the individual stars, though.
- The uncertainties of the metallicities obtained and the small size of the RRL sample (only 4 stars) render the material unsuitable for constructing a MDF and draw conclusions about the history of the SMC.
- From publications in 2011 and 2012, it appears that astronomers such as Efstratios Kapakos et al. and Raoul Haschke et al. has successfully pursued study of RRL metallicities in the SMC, using the Fourier decomposition technique. This kind of study, based on photometry, has been more fruitful than the attempt at multislit spectroscopy presented here.

8 Acknowledgements

Thanks to Thomas Bensby for suggesting this project, providing the raw images and supervising my work, and to Ragnar Bengtsson for being my examiner and for valuable comments. Thanks to Andrew Layden (Bowling Green State University, Ohio, USA) for answering my questions and to Nils Ryde for good discussions and encouragement. Thanks to Ingemar Lundström for reading and commenting on a version of this thesis. Thanks to Andreas Edholm (student opponent) and Dainis Dravins (faculty representative) for questions and comments after my public presentation of this thesis on the 29th of January 2013. Thanks to my office mate Dominika Boneberg for answering my \LaTeX questions and to Stéphane Guisard for giving me permission to use the fine SMC photo. The Astrophysics Data System and Extragalactic Database (NED) of NASA, the SIMBAD Astronomical Database and the GEOS RR Lyrae database (hosted by L'Observatoire Midi Pyrénées) were all useful for this work. I am pleased to acknowledge the generous support of *Stig och Ragna Gorthons stiftelse* in Helsingborg during my years as an undergraduate student.

References

- Baird, S. R., Smith, H. A., Cook, K. H., Keller, S. C., & Walker, A. R. 2011, in American Astronomical Society Meeting Abstracts 218, 334
- Bastian, U. 2009, Gaia – Taking the Galactic Census : The Magellanic Clouds, http://www.rssd.esa.int/SA/GAIA/docs/info_sheets/IN_Magellanic_Clouds.pdf, accessed: January 2013
- Beers, T. C. 1990, AJ, 99, 323
- Bensby, T. 2004, PhD thesis, Lund University
- Böhm-Vitense, E. 1989, Introduction to stellar astrophysics. Vol. 1, Basic stellar observations and data (Cambridge: Cambridge University Press)
- Borissova, J., Minniti, D., Rejkuba, M., Alves, D., Cook, K. H., & Freeman, K. C. 2004, A&A, 423, 97
- Buchheim, R. K. 2007, The sky is your laboratory : advanced astronomy projects for amateurs (Berlin: Springer)
- Clementini, G., Tosi, M., & Merighi, R. 1991, AJ, 101, 2168
- Davenhall, A. C., Privett, G. J., & Taylor, M. B. 2001, The 2-D CCD Data Reduction Cookbook, <http://star-www.rl.ac.uk/docs/sc5.htx/sc5.html>, accessed: December 2012
- Feast, M. W., Laney, C. D., Kinman, T. D., van Leeuwen, F., & Whitelock, P. A. 2008, MNRAS, 386, 2115
- Gray, D. F. 2005, The observation and analysis of stellar photospheres, 3rd edn. (Cambridge: Cambridge Univ. Press)
- Harris, J. & Zaritsky, D. 2004, AJ, 127, 1531
- Haschke, R., Grebel, E. K., Duffau, S., & Jin, S. 2012a, AJ, 143, 48
- Haschke, R., Grebel, E. K., Frebel, A., Duffau, S., Hansen, C. J., & Koch, A. 2012b, AJ, 144, 88
- Hübscher, J., Lange, T., Paschke, A., Vohla, F., & Walter, F. 2005, Open European Journal on Variable Stars, 1, 1
- IMACS. 2008, The IMACS User Manual – Las Campanas Observatory, <http://www.lco.cl/telescopes-information/magellan/instruments/imacs/user-manual/the-imacs-user-manual>, accessed: September 2012
- Kapakos, E., Hatzidimitriou, D., & Soszyński, I. 2011, MNRAS, 415, 1366

- Karttunen, H., Kröger, P., & Oja, H. 2007, *Fundamental Astronomy* (Springer)
- Layden, A. C. 1994, *AJ*, 108, 1016
- Le Borgne, J. F., Klotz, A., & Boer, M. 2004, *Information Bulletin on Variable Stars*, 5568, 1
- Lodders, K., Palme, H., & Gail, H.-P. 2009, *Landolt Börnstein*, 44
- Marín-Franch, A., Aparicio, A., Piotto, G., Rosenberg, A., Chaboyer, B., Sarajedini, A., Siegel, M., Anderson, J., Bedin, L. R., Dotter, A., Hempel, M., King, I., Majewski, S., Milone, A. P., Paust, N., & Reid, I. N. 2009, *ApJ*, 694, 1498
- Matteucci, F. 2001, *The chemical evolution of the galaxy* (Dordrecht: Kluwer)
- Matthews, L. D., Marengo, M., Evans, N. R., & Bono, G. 2012, *ApJ*, 744, 53
- Murdin, P., ed. 2001, *Encyclopedia of Astronomy and Astrophysics*, Vol. 2 – 3, *Encyclopedia of Astronomy and Astrophysics* (Institute of Physics Pub.)
- Pagel, B. E. J. 2009, *Nucleosynthesis and chemical evolution of galaxies*, 2nd edn. (Cambridge, UK: Cambridge University Press)
- Percy, J. R. 2007, *Understanding variable stars* (Cambridge: Cambridge University Press)
- Robinson, K. 2007, *Spectroscopy : The Key to the Stars, Reading the Lines in Stellar Spectra* (London: Springer)
- Sabbi, E., Gallagher, J. S., Tosi, M., Anderson, J., Nota, A., Grebel, E. K., Cignoni, M., Cole, A. A., Da Costa, G. S., Harbeck, D., Glatt, K., & Marconi, M. 2009, *ApJ*, 703, 721
- Samus, N. N., Durlevich, O. V., & et al. 2012, *General Catalogue of Variable Stars*, <http://www.sai.msu.su/gcvs/gcvs/index.htm>, accessed: December 2012
- Sandage, A. 2004, *AJ*, 128, 858
- Smith, H. A. 1995, *RR Lyrae stars* (Cambridge: Cambridge Univ. Press)
- Smith, H. A., Catelan, M., & Clementini, G. 2009, in *American Institute of Physics Conference Series*, Vol. 1170, *American Institute of Physics Conference Series*, ed. J. A. Guzik & P. A. Bradley, 179–187
- Soszyński, I., Udalski, A., Szymański, M. K., Kubiak, J., Pietrzyński, G., Wyrzykowski, L., Ulaczyk, K., & Poleski, R. 2010, *ACTAA*, 60, 165
- Soszyński, I., Udalski, A., Szymanski, M., Kubiak, M., Pietrzynski, G., Wozniak, P., Zebrun, K., Szewczyk, O., & Wyrzykowski, L. 2002, *ACTAA*, 52, 369

- Steer, I. 2012, *Nature*, 490, 176
- Subramanian, S. & Subramaniam, A. 2012, *ApJ*, 744, 128
- van der Marel, R. P., Kallivayalil, N., & Besla, G. 2008, *Proceedings of the International Astronomical Union*, 4, 81
- von Humboldt, A. 1874, *Alexander von Humboldts Kosmos : Entwurf einer physischen Weltbeschreibung*. Bd 3 (Stuttgart: Cotta)
- Walawender, J. 2012, *Introduction to IRAF. VI. Basic Reductions of Spectroscopic Data*, http://www.twilightlandscapes.com/IRAFtutorial/IRAFintro_06.html, accessed: September 2012
- Wallerstein, G., Gomez, T., & Huang, W. 2012, *APSS*, 341, 89
- Wehlau, A. & Hogg, H. S. 1978, *AJ*, 83, 946
- Westerlund, B. E. 1997, *The Magellanic Clouds* (Cambridge: Cambridge Univ. Press)

9 Appendices

9.1 Appendix 1: Supplementary images

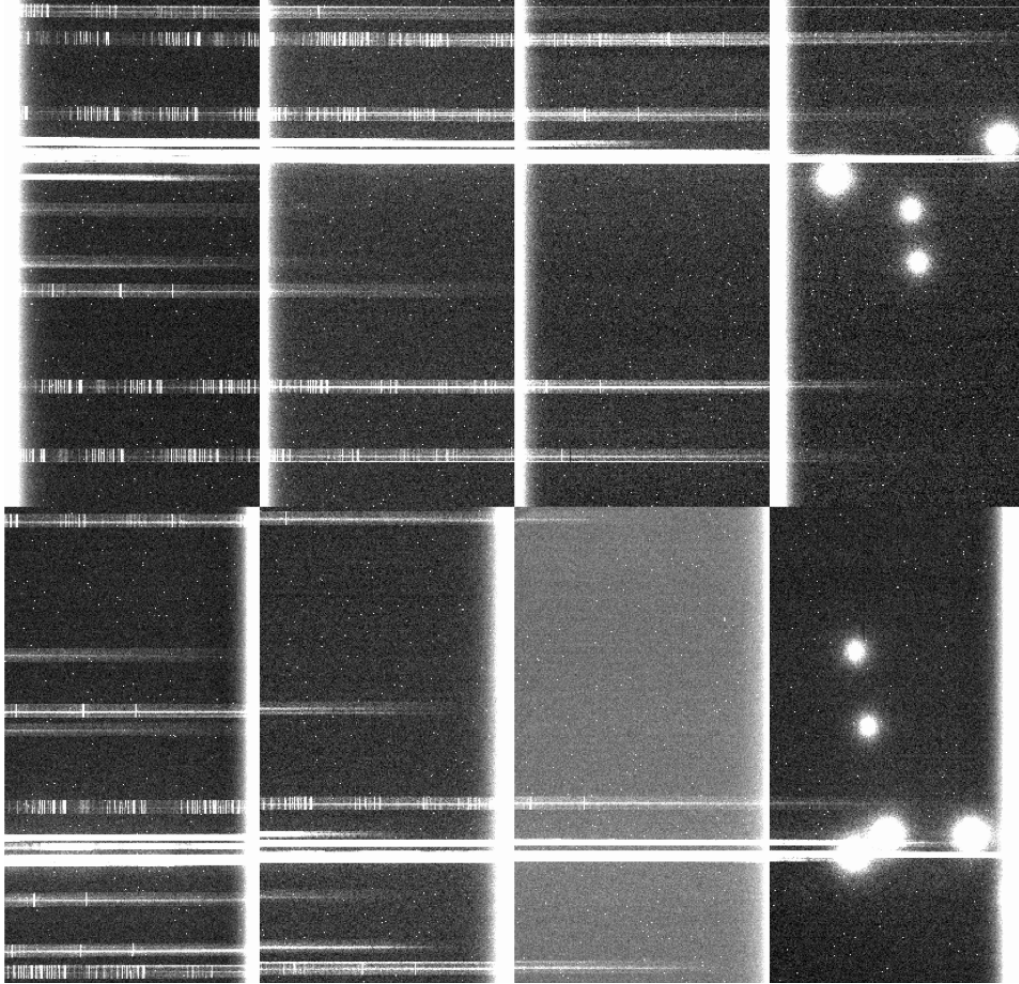


Figure 13: Example image from IMACS taken in multislit mode. This is the spectra from the SMC3 field on 26 September 2005 (UT) in raw format, without cosmic ray hits removed. The bright spots to the right in the image is starlight leaking through the alignment holes of the slitmask. The image is somewhat cropped. The RRL spectra can be seen as stripes extending over several CCD chips.

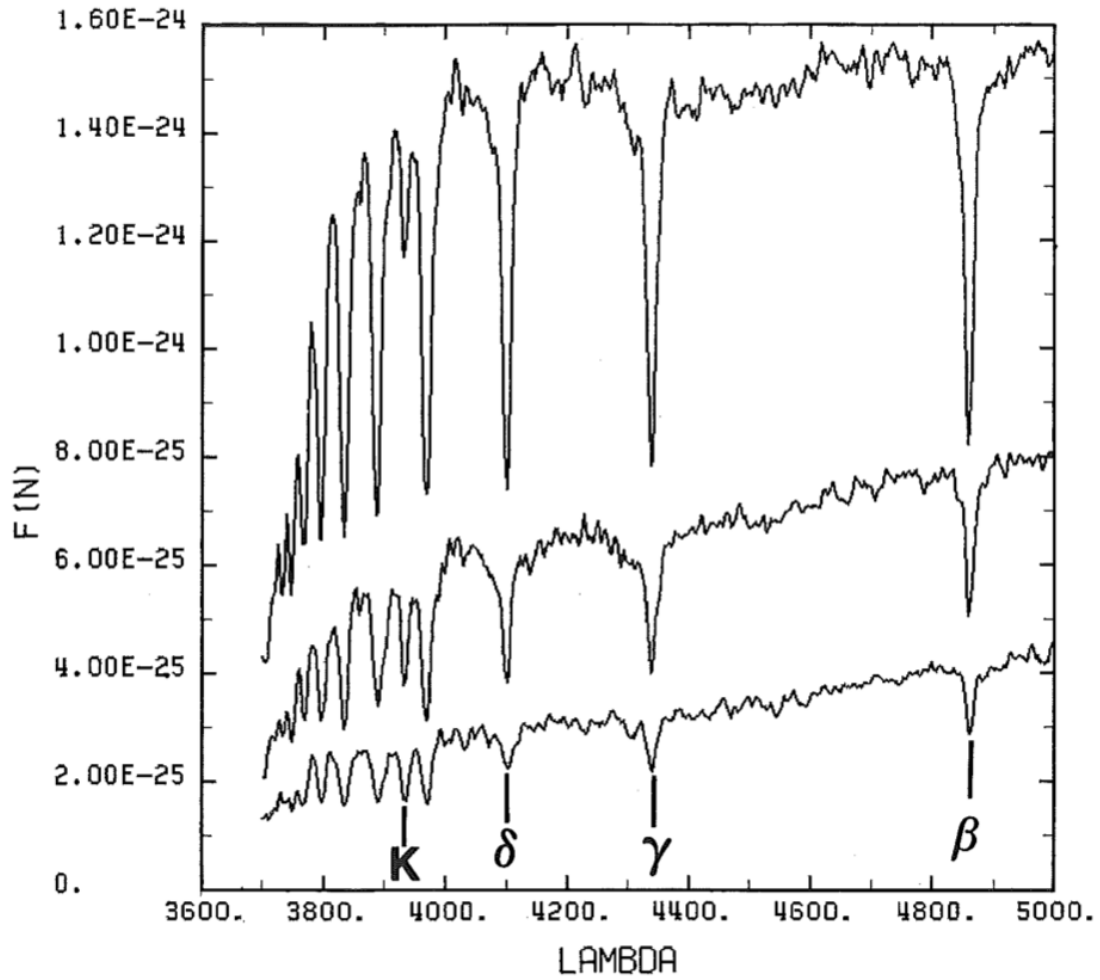


Figure 14: The spectrum of the intermediate metallicity RRL star RW Dra shown from maximum light (top) to minimum light (bottom). The spectral lines used in this work are identified at the bottom. The spectra have been slightly shifted vertically to avoid overlapping. This figure was used as an aid when the lines of the spectra in this work were to be identified. The x axis gives wavelength in \AA and the y axis gives the intensity in arbitrary units. The figure is reproduced from *RR Lyrae Stars* by Smith (1995) with permission from Cambridge University Press.

9.2 Appendix 2: Supplementary method descriptions

Section 4.1 described the main features of the image reduction and spectrum extraction routine. Here, a more detailed description is presented. The processing of the raw FITS images was done as follows:

1. **Labelling the images:** The task CCDHEDIT was used to label all images according to their type, i.e. telling IRAF which image is a bias, a flat field, a comparison arc image or a science image. This information is entered as "imagetype" in the FITS header of the image.
2. **Making master versions of the bias images:** The task ZEROCOMBINE was used to combine bias images into one master bias image per CCD chip. This was done by taking the median values of the pixel values from each bias image to form the master bias image.
3. **Making normalised, smoothed flat field images:** First, the bias was subtracted from all the flat fields and science exposures (but not the arc exposures) using the task IMARITH. Then, all the bias subtracted flat fields for each field of view and chip were median combined using the task COMBINE to produce master flat fields. These master flat fields were then smoothed using the task MEDIAN, to make it possible to produce a normalised master flat field by dividing the bias subtracted flat field with the smoothed flat field with the task IMARITH.
4. **Cropping, applying the flat field and removing cosmic rays from an image:** A considerable (10 - 30 pixels) and unexpected offset between the science exposures and the flat fields had to be compensated for by cropping the flat fields and the science exposures in a suitable way (using the IMCOPY task) before dividing the science exposure with the normalised flat field to obtain a normalised, flat fielded science exposure. Finally, cosmic ray hits and other random pixel errors in the images were removed with the CRMEDIAN task.

Having obtained a bias subtracted, flat fielded science exposure with cosmic ray hits removed, swaths containing the spectrum from one object were copied out of the science exposure (see Figure 7), along with the accompanying arc exposure, using IMCOPY. The extraction of spectra and the application of a wavelength solution was done as follows:

1. **Indicating the direction of dispersion:** In order for IRAF to successfully extract a spectrum, the task for extraction must know the direction of spectral dispersion in the image. This is entered into the FITS header of image using CCDHEDIT.
2. **Setting apertures for the spectrum and the background:** The task APALL displays a window where it is possible to set apertures for the extraction of the spectrum, see Figure 8. One aperture is given where light from the astronomical object is present in the image, and other apertures are given for the background.

APALL also establishes the trace, i.e. the path followed by the aperture as one moves along the dispersion axis. The width of images from which the spectra were extracted is 2050 pixels, and the difference in height for the trace across the width of the image was typically 2 – 5 pixels. A polynomial with a degree between 3 and 7 usually described the trace well.

3. **Generating a wavelength calibration solution:** The task IDENTIFY associates the wavelengths from a line list for the HeNeAr mixture with the lines in the calibration lamp exposure. A window is displayed, showing the lines from the HeNeAr lamp, and by clicking on a the lines and entering their wavelengths from the line list, a wavelength solution can be constructed. As more lines are fitted to the solution, the residuals of the solution is shown after each fit.
4. **Applying the wavelength solution to the spectrum:** The wavelength solution is associated with the science spectrum using the HEDIT task, by adding the keyword REFSPEC1 to the FITS header of the science spectrum. The wavelength solution is finally applied with the DISPCOR task.

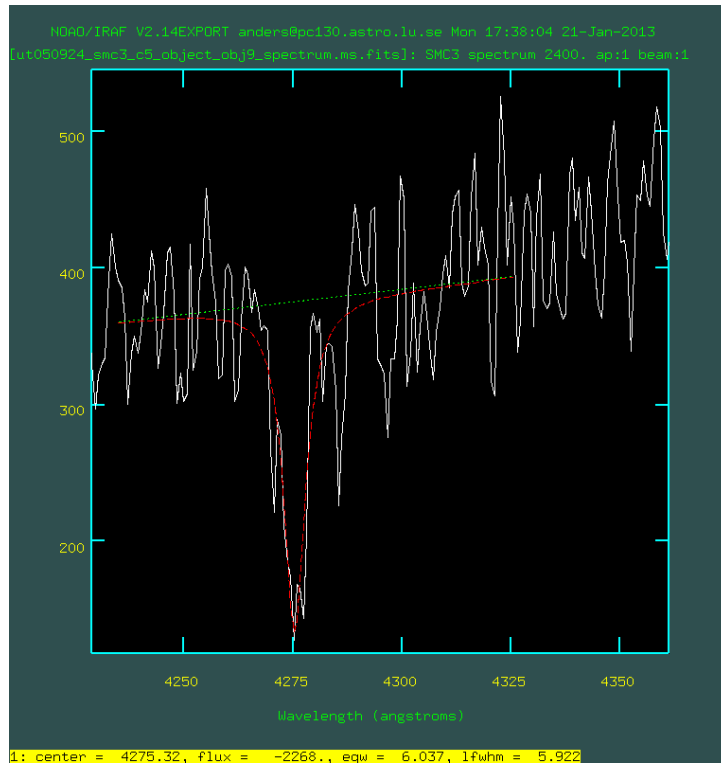


Figure 15: The SPLIT task in IRAF, used to fit a lorentzian profile to the H γ line in the spectrum of SMC_SC3_9362.

9.3 Appendix 3: Supplementary tables

When measuring the EW of a spectral line with IRAF, either a gaussian or a lorentzian profile was fitted to the line. For each line, the profile which gave the seemingly best fit was used.

Table 12: Measured equivalent widths for the standard RRL stars

Object	Balmer β		Balmer γ		Balmer δ		Ca II K	
	λ (Å)	EW (Å)	λ (Å)	EW (Å)	λ (Å)	EW (Å)	λ (Å)	EW (Å)
SV Eri (1)	4594.01	6.9	4072.29	6.011	3836.32	6.409	3669.54	2.031
SV Eri (2)	3966.76	9.445	3461.36	8.6	3237.48	10.15	3082.46	1.28
X Ari	3844.72	7.998	3344.77	8.905	3123.01	10.57	2969.88	0.9094
DX Del	4641.52	8.335	4121.19	8.522	3881.36	9.285	3712.24	4.387

Table 13: Measured equivalent widths for RRL stars in M 22

Object	Balmer β		Balmer γ		Balmer δ		Ca II K	
	λ (Å)	EW (Å)	λ (Å)	EW (Å)	λ (Å)	EW (Å)	λ (Å)	EW (Å)
NGC6656_SAW_V6	4626.66	4.854	4113.59	2.471	3870.7	4.282	3720.78	3.646
NGC6656_SAW_V15	–	–	4107.49	2.661	3868.3	4.377	3695.36	5.368

Table 14: Measured equivalent widths for RRL stars in the SMC

Object	Balmer β		Balmer γ		Balmer δ		Ca II K	
	λ (Å)	EW (Å)	λ (Å)	EW (Å)	λ (Å)	EW (Å)	λ (Å)	EW (Å)
SMC_SC3_28949	4219.08	12.62	3717.97	11.93	3510.64	14.27	3375.21	2.449
SMC_SC3_93692	4796.41	9.354	4275.29	6.314	4036.92	9.134	3869.22	5.721
SMC_SC3_97657	–	–	4241.51	5.41	4033.50	7.942	3933.09	1.622
SMC_SC2_102160	4203.92	9.890	3651.96	9.432	3334.29	11.87	3081.45	5.289

9.4 Appendix 4: A simple model of a pulsating star

While studying the literature on pulsating stars, I found the following way to estimate the pulsation period interesting and elegant, and therefore relate it here.

The analogy of a standing wave on a piece of rope is useful when the mechanism of a pulsating star is to be understood. This example is based on pp. 162-164 in Böhm-Vitense (1989). Consider a rope, attached at one end and free to be moved at the other. By moving the unattached end of the rope up and down at a suitable period, a standing wave travelling back and forth along the rope can be achieved. Similarly, a standing wave travelling inside a star of radius R (where the speed of sound v in the interior of the star is assumed to be the same throughout the star) takes

$$T = 2R/v \quad (14)$$

to travel to the centre of the star and back. Assume that the speed of sound inside the star can be expressed as

$$v = \sqrt{\frac{\gamma P}{\bar{\rho}}} \quad (15)$$

where γ is a constant (the heat capacity ratio), P is the pressure and $\bar{\rho}$ is the density of the star. A rough, order-of-magnitude, approximation of the pressure inside the star can be made with the classical formula for the pressure P exerted by a pillar of material with height h and density $\bar{\rho}$ under the acceleration of gravity g : $P = \bar{\rho}gh$. By assuming that the height of the pillar is the radius R of the star, that the density is the average density $\bar{\rho}$ of the star and that the acceleration of gravity in this case is the surface gravity of the star, an estimate is made. The average density of a star with mass M is given by $\bar{\rho} = \frac{3M}{4\pi R^3}$ and the surface gravity is given by

$$g = \frac{GM}{R^2} \quad (16)$$

Let us now insert the expression for the speed of sound in equation 15 into equation 14 and substitute $P = \bar{\rho}gR$ for pressure:

$$T = \frac{2R}{v} = 2R\sqrt{\frac{\bar{\rho}}{\gamma P}} = 2R\sqrt{\frac{\bar{\rho}}{\gamma\bar{\rho}gR}} = 2\sqrt{\frac{R}{\gamma g}}.$$

Substitution of equation 16 for the acceleration of gravity and use of the density relation $\frac{R^3}{M} = \frac{3}{4\pi\bar{\rho}}$ gives us

$$T = 2\sqrt{\frac{R}{\gamma g}} = 2\sqrt{\frac{R^3}{\gamma GM}} = 2\sqrt{\frac{3}{\gamma G 4\pi\bar{\rho}}}.$$

Assuming that the gas in the star is a monatomic ideal gas means that $\gamma = 5/3$ which gives us the factor $2\sqrt{\frac{3}{\gamma 4\pi}} \approx 0.76$ in the above expression. If this factor is assumed to

be ~ 1 , we obtain the expression

$$T \approx \frac{1}{\sqrt{G\bar{\rho}}} \quad (17)$$

for estimating the pulsation period of the star. A unit check reveals that this expression gives a result with the unit time. This is a rough estimate, reached via a number of approximations. In the literature, this relation is often written as $T \propto \bar{\rho}^{-1/2}$, which is more general than the way it is given in equation 17.

Using typical values for the radius and mass of a RR Lyrae star¹³ ($R \approx 5 R_{\odot}$ and $M \approx 0.7 M_{\odot}$) the pulsation period $T \approx 4 \cdot 10^4$ s, i.e. about 0.5 days, is obtained from equation 17. This is a good estimate of the pulsation period of a RR Lyrae¹⁴ star (which typically can be 0.2 - 1.1 days), considering the many approximations. To further check the validity of equation 17, it can be applied to a larger and more massive type of pulsating variable star, the Cepheids. Assuming that the mass and radius of the prototype star, δ Cephei ($R \approx 45 R_{\odot}$ and $M \approx 5 M_{\odot}$)¹⁵, are representative for this type of pulsator, the pulsation period is estimated to be $T \approx 4 \cdot 10^5$ s, i.e. about 5 days. This happens to agree quite well with the pulsation period of δ Cephei, and is of the right order of magnitude for other Cepheids.

This use of equation 17 gives acceptable order-of-magnitude estimates of pulsation periods. It also appears to tell us that the analogy with the standing wave on the rope can say something about how a pulsating star works. The time of travel for a standing wave inside a pulsating star seems to agree quite well with the pulsation period, and stellar pulsation appears to be a resonance phenomenon.

¹³From Table 1.1 in Smith (1995).

¹⁴Astronomy is (in)famous for its profusion of different naming conventions. The following convention is used for variable stars: The variable stars in a certain constellation are designated R, S, T . . . Z together with the genitive case of the constellation name for the 9 brightest variables in the constellation. After that, pairs of letters (RR, RS . . . RZ, SS, ST . . . etc. to ZZ) and then AA, AB . . . AZ, BB . . . BZ up to QZ (omitting J) gives another $\sum_{i=1}^{25} i = 325$ combinations. This gives $9 + 325 = 334$ possible names in this style. Beyond this number, variables in a constellation are designated V335, V336 etc. This explains a name such as RR Lyrae (or, abbreviated, RR Lyr).

¹⁵From Table 1 in Matthews et al. (2012).

10 Populärvetenskaplig sammanfattning på svenska

Otåliga stjärnor och metall? – Avtryck i den kosmiska historien.

Har man kosmiska frågor kan man med fördel vända sig till drängen, sjömannen och diktaren Harry Martinson. Förutom i hans *Aniara* har intryck från astronomin och dess världsbild satt spår på många håll i hans diktning. Dikten *Solen* ur samlingen *Gräsen i Thule* från 1958 innehåller, om man ger sin fantasi litet svängrum, råmaterialet till detta examensarbete.

SOLEN

*Solen är en het juvel
som aldrig är nöjd med sin hetta och glans.
Flammande otålig blixtrar den hårt
mot gud sin guldsmed.*

Otåliga stjärnor och metall är just vad detta examensarbete har handlat om. De otåliga – eller, som en astronom skulle säga: variabla – stjärnorna är av en typ som kallas för RR Lyrae-stjärnor. Den metall det handlat om är inte, som hos Martinson, guld utan järn. Den fråga det handlat om har varit hur Lilla magellanska molnet (en granngalax till vår egen galax Vintergatan) utvecklats, och hur RR Lyrae-stjärnorna kan användas som markörer för att undersöka ett tidigt skede av denna utveckling. I undersökningen har spektra (ljus uppdelat efter våglängd) av RR Lyrae-stjärnor i Lilla magellanska molnet använts för att bestämma hur mycket järn stjärnorna innehåller. Det är intressant att undersöka eftersom varje generation av stjärnor framställer tunga grundämnen (som t.ex. järn), och tidiga stjärngenerationer därför borde ha lägre halter av tunga grundämnen. RR Lyrae-stjärnorna i Lilla magellanska molnet antas tillhöra de tidiga stjärngenerationerna, och en undersökning av just hur hög (eller, snarare, låg) halt av tunga grundämnen dessa stjärnor har kan ge ett prov på hur Lilla magellanska molnets tidiga historia såg ut. För att förstå hur detta arbete gått till skadar det inte att känna till litet mer om stjärnors kemiska utveckling, Lilla magellanska molnet, RR Lyrae-stjärnor och spektroskopi.

Vår hemplanet, Jorden, kretsar runt Solen, som är en rätt omärklig stjärna i vår hemgalax, Vintergatan. Klara och mörka nätter kan man förnimma ett ljussvagt, molnliknande stråk över stjärnhimlen – detta stråk är Vintergatan, sedd inifrån. Galaxen är en vidsträckt, platt skiva vars synliga innehåll är i storleksordningen 100 miljarder stjärnor samt mängder av gas och stoft. Det tar ljuset ungefär 100 000 år att färdas från den ena sidan av Vintergatan till den andra; dess diameter är alltså 100 000 ljusår. Vintergatan präglas av sin spiralstruktur, som innebär att mycket av stjärnorna, gasen och stoftet i galaxen är koncentrerat till fyra spiralarmar som sträcker sig ut från galaxens centrum.

Vintergatan har en kemisk uppdelning som kan säga oss något om dess historia. Den-

na kemiska uppdelning kännetecknas av fördelningen av metaller, och lägg märke till att astronomin har för vana att räkna alla grundämnen tyngre än helium som metaller. Exempel på detta är att de inre delarna av Vintergatans skiva innehåller många yngre stjärnor med högre metallhalt än de äldre stjärnor som finns i bl.a. den tunna svärm av stjärnor som omger hela galaxen. Orsaken till att stjärnor av olika åldrar har olika metallhalt är det sätt som stjärnor bildas, lever och dör på. En stjärna bildas ur den gas och det stoft som finns i rymden mellan stjärnorna, och består mest av de lättaste grundämnena – väte och helium – med en liten andel tyngre grundämnen. När universum bildades fanns nästan uteslutande väte och helium, och de tyngre grundämnena har senare bildats i generationer av stjärnor. Tyngre grundämnen bildas i det som är stjärnornas energikälla: fusion. I det täta och varma inre av en stjärna kan fusion, eller sammanslagning, av lättare grundämnen till tyngre ske – då avges också energi, som får stjärnan att lysa.

En stjärnas livslängd avgörs främst av dess massa. Solen har en sammanlagd livslängd på drygt tio miljarder år, medan en jättestjärna med tio gånger solens massa har en livslängd på ungefär tio miljoner år. Sättet som stjärnan dör på avgörs också av dess massa. En sollik stjärna kastar mot slutet av sitt liv ut ungefär hälften av sitt materiere innehåll i en s.k. planetarisk nebulosa. En sådan händelse är långt mer beskedlig än det sätt som en jättestjärna dör på; en massiv stjärna slutar sitt liv som supernova, då det mesta av stjärnan kastas ut i rymden i en våldsam explosion. En sollik stjärna slutar genom en lätt hostning, en massiv stjärna genom en rejäl nysning! Detta stellära hostande och nysande svarar för att rymden mellan stjärnorna ständigt berikas med tunga grundämnen, och är orsaken till att yngre (senare generationers) stjärnor har högre halt av tunga grundämnen än äldre (tidigare generationers) stjärnor.

Således kan skillnaden i halt av tunga grundämnen i olika delar av Vintergatan säga oss något om de olika delarnas historia. Den kemiska utveckling som sker i Vintergatan sker också i andra galaxer, och genom att studera metallfattiga – och förment gamla – stjärnor kan man dra slutsatser om galaxernas tidigaste historia.

Lilla magellanska molnet är den galax vi skall intressera oss för här. Vintergatan har som följeslagare ett antal mindre galaxer i sin närhet; de största två kallas för de Magellanska molnen, och de är synliga för blotta ögat från södra halvklotet, som mindre dimfläckar på himlen. Den persiske 900-talsastronomen Abd al-Rahman al-Sufi var troligen den förste att i skrift nämna det Stora magellanska molnet. Molnen blev allmänt kända i Europa efter de stora upptäcktsresorna till sjöss under 1500-talets början, då bland andra Fernão de Magalhães lade märke till dem – därav namnen.

De Magellanska molnen är oregelbundna dvärggalaxer utan den tydliga spiralstruktur som finns i Vintergatan. Det Stora molnet är större i både absolut och skenbar mening, beläget på ett avstånd av ungefär 160 000 ljusår och med en massa på ungefär 10 miljarder solmassor. Det Lilla molnet ligger ungefär 200 000 ljusår ifrån oss och har en massa på ungefär 1 miljard solmassor. Lilla molnet ligger alltså på ungefär 1/13 av avståndet till vår närmaste, stora galaxgranne, Andromedagalaxen (som kan ses för blotta ögat på norra stjärnhimlen). Låter vi i tanken Malmö (ytmässigt) representera

Vintergatan markeras Lilla magellanska molnets läge ungefär av Svedala, på ett kosmiskt Söderslätt.

Närheten till de Magellanska molnen gör dem till tacksamma objekt att studera, och de kan ge oss viktiga insikter i hur galaxer är uppbyggda och utvecklas. Dessutom är de två Molnen viktiga steg på den kosmiska avståndsskalan, och mätning av avstånden till dem kan påverka mätningar till andra, långt mer avlägsna galaxer.

De Magellanska molnen är flitigt studerade – och livligt debatterade. Olika slutsatser har nåtts om t.ex. deras rörelse. Vissa hävdar att Molnen gör sin första passage i Vintergatans närhet, andra att de kretsar runt Vintergatan med omloppstider på flera miljarder år.

För Lilla molnets del tyder det mesta på att det har en utsträckning i riktning mot oss och Vintergatan; detta är troligen en följd av att tidvattenkrafter tänjt ut Lilla molnet. Medan bredden och höjden är lätt att mäta direkt på himlavalvet är längden omstridd. En annan omstridd fråga är Lilla molnets stjärnbildningshistoria. Den senaste årmiljarden verkar ha präglats av livlig stjärnbildning, medan åsikterna går isär när det gäller den tidiga historien: En studie av över 6 miljoner stjärnor i Molnet har fått en grupp astronomer att dra slutsatsen att många stjärnor bildades för över 8 miljarder år sedan, medan en annan grupp hävdar att den tidiga stjärnbildningen i Lilla molnet var rätt såvlig. Därför är det angeläget att försöka ta reda på mer om Lilla molnets tidiga historia. Hur gör man det? Jo, genom att fråga någon som var med när det begav sig!

Då hade det inte ens räckt med Astronomiska Sällskapet Tycho Brahes äldsta medlem, Greta Andersson (1902-2012) i Helsingborg. Det vore bra att för ändamålet studera någon typ av stjärna som är ca 10 miljarder år gammal, och som man kan veta har åldern inne. Sådana stjärnor finns, och de kallas RR Lyrae-stjärnor. Det är en typ av stjärna som inte uppför sig så beskedligt som vår sol, utan pulserar och ändrar ljusstyrka med en period som kan vara från någon timme till upp mot ett dygn. Den skenbart ljusaste variabla stjärnan av denna typ på himlen, RR Lyrae själv, kan man betrakta med fältkikare i stjärnbilden Lyran, nära gränsen till stjärnbilden Svanen.

I solen och många andra stjärnor råder en balans mellan den inåtriktade tyngdkraften och den utåtriktade strålningskraften som får dem att vara stabila. RR Lyrae-stjärnor, däremot, har lämnat detta stabila skede och har börjat pulsera. Teorin om stjärnors utveckling säger att en stjärna med en massa på ungefär 0,8 solmassor efter 10 miljarder år av stabilitet träder in i ett pulserande tillstånd, och tillbringar ungefär 100 miljoner år med att pulsera. RR Lyrae-stjärnor har ett mycket karakteristiskt sätt att pulsera på, och de är på så vis lätta att identifiera. Om man överhuvudtaget hittar RR Lyrae-stjärnor i en grupp av stjärnor eller en galax visar det att gruppen eller galaxen måste vara minst 10 miljarder år gammal, och genom att undersöka metallhalten i RR Lyrae-stjärnor (som, i kraft av deras ålder, bör vara tämligen låg) kan man få reda hur fördelningen av tunga grundämnen såg ut tidigt i galaxens historia. Det man söker kallas på astronomiskt fikonspråk för *metallicitetsfördelningsfunktion*.

I en sådan undersökning används metallen järn som markör för förekomsten av tunga grundämnen. Astronomin använder beteckningssättet $[\text{Fe}/\text{H}]$ för att beteckna en stjärnas järninnehåll relativt solen. Man anger då hur många väteatomer (H) det finns för varje järnatom (Fe). En stjärna med $[\text{Fe}/\text{H}] = 0$ har på denna skala samma järnhalt som solen, alltså en ganska hög halt. RR Lyrae-stjärnor förväntas ha järninnehåll från $[\text{Fe}/\text{H}] = 0$ till $[\text{Fe}/\text{H}] = -2$. Skalan är logaritmisk, och logaritmer är matematiska funktioner som underlättar hantering av små och stora tal. Följande tabell kan hjälpa till att ge en uppfattning om hur skalan fungerar:

Tabell 15: Vad betyder $[\text{Fe}/\text{H}]$?

$[\text{Fe}/\text{H}]$	Väteatomer per järnatom i stjärnan
0	35 000
-1	350 000
-2	3 500 000

Små förändringar i $[\text{Fe}/\text{H}]$ innebär alltså stora skillnader i järnförekomst. För varje heltalssteg i $[\text{Fe}/\text{H}]$ ändras antalet väteatomer med en faktor 10; den matematiskt intresserade läsaren anar här, mycket riktigt, att det hela bygger på 10-logaritmer.

Vi har nu gått igenom **VAD?** (nämligen Lilla magellanska molnets tidiga historia, studerad med RR Lyrae-stjärnor som markörer) och **VARFÖR?** (för att få reda på mer om Lilla magellanska molnets tidiga historia, som är högtintressant eftersom Molnet är en närbelägen och ganska lättstuderad galaxgranne). Då återstår **HUR?**, och det handgripliga arbete som jag utfört under examensarbetet på Lunds observatorium under perioden september 2012 – januari 2013.

Att ta reda på en stjärnas sammansättning (däribland dess järnhalt) gör man lättast med hjälp av ett spektrum av stjärnan. Ett spektrum av ljus innebär att ljuset delas upp efter våglängd. Det mest kända exemplet är troligen regnbågen, där vattendroppar i atmosfären reflekterar och bryter upp solljuset i dess bestånds färger från långvågigt, rött (via bl.a. en sådan försummad färg som indigo) till kortvågigt, violett. Om man med hjälp av en spektrograf, där antingen ett prisma eller ett gitter bryter upp ljuset, delar upp solens ljus i ett spektrum kommer man att se ett antal mörka linjer i det. Dessa linjer, som varit kända sedan 1800-talets början, orsakas av att olika ämnen i solens yttre delar absorberar ljus vid bestämda våglängder. Genom att jämföra dessa s.k. absorptionslinjer i solspektrum med motsvarande linjer i laboratorieförsök kan man alltså identifiera vilka grundämnen som finns på solen. Detta gäller även för andra stjärnor.

Nästa steg är att ta reda på hur mycket av ett visst ämne som förekommer i en stjärna. När man granskar hur intensiv en absorptionslinje är visar det sig att dess

intensitetsfördelning inte är obegränsat smal. Den är heller inte rektangelformad, utan har snarare en form som påminner om en tratt som vidgas uppåt – den har en kärna, och vingar åt sidorna. Genom att i spektrum mäta vilken yta denna linjeprofil tar upp kan man, genom sinnrika beräkningar, komma fram till hur mycket av det ämne som orsakat linjen som finns i stjärnan.

En version av denna metodik användes i examensarbetet. Den amerikanske astronomen Andrew Layden publicerade 1994 en stor studie av bl.a. metallhalt i 302 RR Lyrae-stjärnor i Vintergatan. För denna undersökning hade han utvecklat en metod som använde en kalcium-linje och tre väte-linjer i ett RR Lyrae-spektrum för att bestämma järnhalten. Det kan verka besynnerligt att inte använda en järnlinje direkt, men flera undersökningar har visat att kalciumlinjerna är väl ägnade för järnmätningar och dessutom är kalcium- och vätelinjer mycket starkare i spektrum än järnlinjerna. Laydens metod kom till användning i mitt arbete.

Min handledare, Thomas Bensby, och hans kollega Sally Oey genomförde i september 2005 en tre nätters observationskampanj vid 6,5-meterteleskopet Magellan I i Chile. På detta teleskop finns en spektrograf och kamera som heter IMACS, och genom att rikta teleskopet mot olika områden i Lilla magellanska molnet och låta ljuset falla genom en mask med hål i – hål belägna där man på förhand visste att en RR Lyrae-stjärna skulle befinna sig – kunde man i en enda exponering med IMACS fånga spektra av över 10 RR Lyrae-stjärnor åt gången.

Min första uppgift under hösten 2012 var att behandla detta material, och utföra hantverket för att gå från råa, obehandlade bilder till stjärnspektra försedda med lämpliga skalor. För detta arbete användes ett datorprogram som heter IRAF – liksom jag ett barn av 1980-talets mitt, men vidareutvecklat genom åren. Sedan var uppgiften att göra mätningar i spektra för att göra det möjligt att beräkna metallhalter. Hur gick det?

Efter att ha behandlat bilder från två nätter av tre stod det klart att materialet inte höll den kvalitet vi hoppats på. I de flesta spektra gick det inte att se några absorptionslinjer alls, däremot mycket brus. RR Lyrae-stjärnorna i Lilla magellanska molnet hade helt enkelt varit för ljussvaga för det teleskop och den exponeringstid som använts. Av de potentiellt ca femtio stjärnor som kunnat ge en metallhaltsbestämning var det bara fyra som var möjliga att mäta. De visade sig ha järnhalter som man kan vänta sig för RR Lyrae-stjärnor, men med ganska stora fel i bestämningarna. Den ursprungliga frågan, om Lilla molnets tidiga historia, går alltså inte att besvara med detta material.

Andra astronomer, bl.a. Efstratios Kapakos i Grekland och Raoul Haschke i Tyskland, har sedan 2005 med andra metoder lyckats bestämma metallhalter för RR Lyrae-stjärnor i Lilla molnet. Astronomin som vetenskap lider alltså inte av att just denna undersökning inte gick att ro i land. Vidare funderingar på järnförekomsten i andra galaxer kan med fördel ske över en tallrik god svartsoppa (rik och flyktig i smaken)¹⁶, vars järnhalt man kan förvissa sig om på helt andra sätt än när det gäller astronomiska objekt.

¹⁶Som t.ex. den svartsoppa hornisten Magnus Hellberg i Musikalliansen Alte Kamereren brukar laga till nämnda orkesters gåsamiddagar.